NTNU
Norwegian University of Science and Technology
Department of Marine Technology

M.Sc.THESIS

Title:	**Delivered:**
Thrust loss on azimuthing thrusters due to Coanda Effect	11.06.10
	Availability:
Student:	**Number of pages:**
Henrik Fjørtoft	91

Abstract:

This master's thesis seeks to investigate "Thrust loss on azimuthing thrusters due to Coanda effect". The Coanda effect is a thruster interaction effect which tends to attract the thruster race towards nearby boundaries and walls. The main objective is to gain knowledge of which conditions are more exposed for the Coanda effect than others.

The approach for investigating the Coanda effect is to measure the effect experimentally. An experiment in NTNU's Marine Cybernetics Lab has been planned and carried out with a focus of measuring the non dimensional thrust loss for different variations of parameters. Parameters investigated is horizontal distance from thruster to model side, vertical distance from thruster to model bottom, downwards tilting of thruster and variation of thrust force.

A mathematical model is made for comparing and verification of results. The mathematical model has proven accurate in predictiong the attachment length of a jet stream.

Experimental results show that both vertical and horizontal variations can reduce the thrust loss due to Coanda effect. The results also show that tilting of the thruster nozzle is very effective in reducing the thrust loss.

Keyword:

Thrust loss
Coanda effect

Advisor:

Professor Sverre Steen

Address:
NTNU
Department of Marine Technology
N-7491 Trondheim

Location
Marinteknisk Senter
O. Nielsens vei 10

Tel. +47 73 595501
Fax +47 73 595697

NTNU Trondheim
Norwegian University of Science and Technology
Faculty of Engineering Science and Technology
Department of MarineTechnology

M.Sc. thesis 2010

for

Henrik Fjørtoft

Thrust loss on azimuthing thrusters due to Coanda effect

Azimuthing thrusters are frequently applied on offshore ships and various specialized vessels to provide good dynamic positioning capability and low-speed maneuverability. However, it is known that the net thrust produced by each thruster might be much smaller than the actual thrust on the unit, due to interaction with the hull and possibly with other thrusters. One of the important physical mechanisms leading to such thrust loss is Coanda effect – when the propeller slipstream attaches to the hull and is re-directed by hull curvature. It is important to have a good knowledge about the relation between the thrust loss due to Coanda effect and important parameters such as thruster loading, distance from hull, distance to bilge, bilge radius, and possibly mounting the thruster so that the thruster propeller axis is pointing slightly downwards, away from the hull. An idea that shall be explored in this thesis is to tilt the duct downwards, rather than tilting the propeller axis.

On this background, the student shall do the following in the master thesis:

1. Give an detailed overview of existing available experimental data (Thon, Lofterød)
2. Make a mathematical model of Coanda effect from propeller slip streams.
3. Plan and perform model tests with an azimuthing thruster. Variation of duct tilt angle shall be one of the investigated parameters.
4. Analyse the experimental results, and compare with the results of the mathematical model – as far as possible.
5. Give recommendations regarding use of duct tilt to reduce Coanda effect for an azimuthing thruster below a flat bottom.

The candidate should in his report give a personal contribution to the solution of the problem formulated in this text. All assumptions and conclusions must be supported by mathematical models and/or references to physical effects in a logical manner.
The candidate should apply all available sources to find relevant literature and information on the actual problem.

The report should be well organised and give a clear presentation of the work and all conclusions. It is important that the text is well written and that tables and figures are used to support the verbal presentation. The report should be complete, but still as short as possible.

The final report must contain this text, an acknowledgement, summary, main body, conclusions, suggestions for further work, symbol list, references and appendices. All figures, tables and equations must be identified by numbers. References should be given by author and year in the text, and presented alphabetically in the reference list. The report must be submitted in two copies unless otherwise has been agreed with the supervisor.

The supervisor may require that the candidate should give a written plan that describes the progress of the work after having received this text. The plan may contain a table of content for the report and also assumed use of computer resources.

From the report it should be possible to identify the work carried out by the candidate and what has been found in the available literature. It is important to give references to the original source for theories and experimental results.

The report must be signed by the candidate, include this text, appear as a paperback, and - if needed - have a separate enclosure (binder, diskette or CD-ROM) with additional material.

Supervisor at NTNU is professor Sverre Steen
Advisors are Øyvind Gjerde Kamsvåg and Noel Dunstan

Supervisor : Professor Sverre Steen
Start : 18.01.2010
Deadline : 06.06.2010

Trondheim, 18.01.2010

Sverre Steen
Supervisor

Summary

The main objectives in this master's thesis is to investigate how the Coanda effect influences a thruster jet which further causes a thrust loss.

The tendency of a thruster slipstream to be deflected towards a nearby surface, for most practical situations the hull of a vessel, is called the Coanda effect and is likely to produce a significant thrust loss under certain geometric conditions.

The approach in this master's thesis is to perform an experiment measuring the direct thrust loss related to the deflection of the slipstream. Results from the experiment are presented along with comparisons with similar experimental results and predicted results acquired from mathematical model. The mathematical model has proven accurate in predicting the deflection of the thruster jet.

Results show that both distances from the thruster to the hull have an influence on the results, and in particular the tilting of the thruster nozzle. The greatest thrust loss measured in the experiment is approximately 25 % loss, which during for example critical offshore operations is significant and may lead to dangerous situations. Variations in thrust force, however, do not represent thrust loss variations according to the experimental results within the specified thrust range. Increasing the distance between thruster and hull bottom reduces the thrust loss with approximately 5 %.

By tilting the thruster downwards 7.5° one can reduce the thrust loss due to Coanda effect with approximately $10 - 15$ %. Analyses show that tilting the thruster farther than 7.5° does not result in a reduced thrust loss, and is not advised as a counter measure for the Coanda effect.

Acknowledgements

This master's thesis could not have been competed without the kind help of personnel related to the Department of Marine Technology at NTNU or of MARINTEK. I would also like to thank Rolls-Royce University Technology Center for creating this assignment and opportunity in the first place. Special contributors which deserves extra credit are:

Anders Lofterød, who has written a master's thesis on the Coanda effect in 2007, has provided valuable information through the experienced learned from his own experiment.

Thanks goes to professor Odd M. Faltinsen who, through conversations, has provided me with valuable insight in the complex mechanisms of the Coanda effect and has kindly offered private notes describing a mathematical method related to the Coanda effect.

Thanks goes to Erik Lehn and Leif Vartdal for valuable advice through conversations on current counter measures against thrust loss due to Coanda effect as well as their reflections on relevant parameters for further work.

Special thanks to department engineer Torgeir Wahl for extraordinary technical assistance related to the performance of the experiment. Special thanks also goes to personnel at MARINTEK involved in the making of the model.

A very special thanks goes to my supervisor, professor Sverre Steen, who has encouraged me to write a master's thesis on this subject and assisted with vital knowledge and experience throughout the planning, executing and post-work analyses of the experiment.

Contents

List of Figures

List of Tables

Chapter 1

Introduction

This master's thesis is an experimental hydrodynamics approach for gaining knowledge on the Coanda effect. The main objective is to perform an experiment, analyze the results in relation with the specified parameter combinations and compare the results with similar experiments and mathematical models. The master's thesis assignment is made through a collaboration between NTNU and Rolls-Royce University Technology Center "Performance in a Seaway".

The Coanda effect is the tendency of a jet stream, when in the vicinity of a solid wall or curved surface, to be deflected from its original path towards the boundary and thus reaching it after a significantly shorter distance than the natural spreading of the jet would cause. The nature of a turbulent jet stream is complex, and no numerical method has proven completely accurate in predicting neither the attachment of jet stream and boundary nor the thrust loss related to it. Experimental studies are therefore of great importance for evaluating mathematical methods and for observations of the nature of the Coanda effect.

A thorough literature study on existing experimental results and mathematical predictions on the Coanda effect is emphasized, and is a significant part of this master's thesis. The main part, however, is the processing of acquired results and comparisons with existing results of similar experimental setup.

Chapter 2

Previous experimental work

The physical behavior of a current being deflected towards a body was first mentioned in literature with Young in mid 1800, according to Fernholz and Willie (1965), and later by Reynolds in 1870, according to Fernholz (1971). The next big leap in knowledge on the Coanda effect came with Henri Marie Coanda (1886-1972), who made new discoveries culminating in a patent for a "Method and apparatus for deviation of a fluid into another fluid" in 1934. Henri Coanda worked within the aeronautical industry and built the worlds first jet aircraft, according to Slomski and Marino. The Coanda effect is highly related to the lift on wings and airfoils (Discovery Channel), and has been explored increasingly along with the rise of the aircraft industry in the post war period. The naval industry first caught interest in the Coanda effect late in this period with the introduction of more complex propulsion systems and the increasing use of foil shaped propeller blades.

Three contributors to the experimental research of the Coanda effect within the naval industry in recent years are Lehn, Thon and Lofterød, all related to MARINTEK and NTNU. These three have performed experiments with partial or full focus on the Coanda effect, and their work and experimental results will be looked more closely into later in this chapter. Lehn (1985), Thon (1986) and Lofterød (2007) will also be used for a comparison with the results from this master's thesis.

2.1 Lehn's experiment

Lehn (1985) published "On the propeller race interaction effects" in 1985 which contained investigations of thruster interaction effects, herein also the Coanda effect. The experiment was performed in Towing Tank no. II at MARINTEK, a neighboring tank to the MCLab where this master's thesis' model test has been carried out. The building materials for Lehns model was waterproof plywood, as for the building materials of this model, although the paint covering both models is most likely of a different character. The model setup of Lehn is shown in 2.1. As for the model test Lehn also measured the total force on the model and the thruster force with two force transducers as a basis for evaluating the Coanda effect. The locations of the force transducers are also shown in 2.1.

Lehn's pontoon shaped model, with a length, breadth and height of $L = 0.8$ m, $B = 0.6$ m and $H = 0.6$ m respectively, in addition to the thruster is shown in 2.1. Lehn's constant parameters and variation parameters with ranges are:

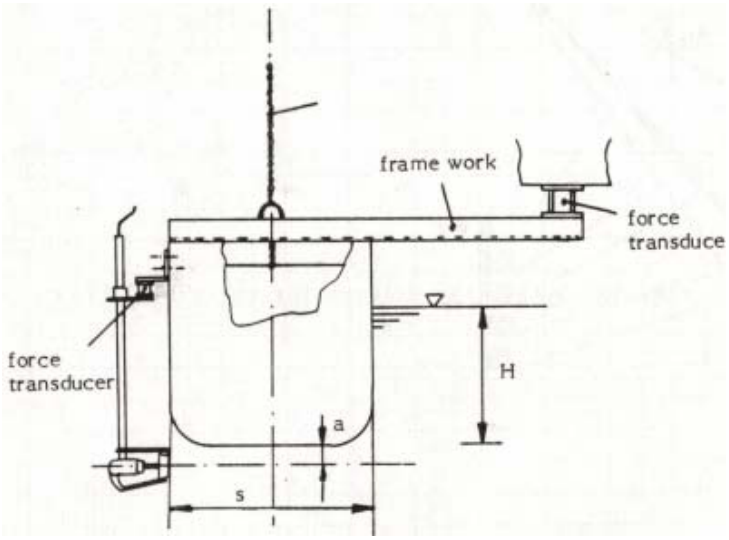

Figure 2.1: Lehns model setup

- Thruster diameter, $D = 0.08$ m
- Constant distance between thruster and pontoon side, $S/D = 7.5$
- Variation of distance between hull bottom and centerline of the thruster, $a/D = 0.9 - 1.9$
- Variation of radius, $R/D = 0 - 1.5$
- Variation of draught, $H/D \approx 1.0 - 5.25$

The experimental results from Lehn's investigation of the Coanda effect along with an explanatory sketch are found in B.1. The results related to the vertical distance between thruster and hull will be commented further in 9.2. From Lehns results it is also possible to extract an expected Coanda thrust loss due to bilge radius of approximately 4 % for a bilge radius of $R = 0.5 \cdot D$. In addition there is an expected Coanda thrust loss due to draught of approximately 4 % for a draught of $H = 1.73 \cdot D$. Lehn concludes that there is a clear tendency that the thrust loss increases with a decreasing distance between the hull and the thruster. Lehn further concludes:

> Due to the Coanda effect a bilge radius of one propeller diameter will deflect the propeller race approximately $2 - 4$ % in vertical direction and result in a thrust loss of 5 %. With a sharp corner there will be no losses.

2.2 Thon's experiment

Thon (1986) published "Deflection of propeller slipstream" in 1986 which contains investigations of what influence a parallel wall or nearby surface have on a propeller slipstream. Thon's experiment was performed in the same towing tank as Lehn's experiment and is divided into two parts. Part one seeks to visualize the slipstream for comparison with observed deflection and a mathematical model. Part two seeks to find the deflection of the slipstream around a curved surface. Part two of Thon's experiment is the most relevant part for comparison of $(1-t)$ in this master's thesis, but part one is relevant when evaluating the attachment length of the thruster race. Part one will be discussed further in 9.3, and figures and data is available in B.2. All

figures in this section are collected from Thon (1986). The properties of the ducted propeller used in Thon's experiment are given in 2.1, and the test conditions for part two is shown in 2.2. Explanatory sketches of symbols and parameters related to Thon's experiment can also be found in B.2.

Propeller diameter	0.08 meter
Number of blades	3
Rate of revolutions	23 rps
Total thrust	9 newton

Table 2.1: Thon's propeller properties

H = 0.48 [m] or 6*D
R = 0.375, 6.25, 9.0, 12.5 [10^{-2} m]
or R/D = 0, 0.47, 0.78, 1.13, 1.56
S/D = 4.7 and 7.6

Figure 2.2: Test conditions for part two in Thon's experiment

As can be seen in B.7 Thon varied the parameters bilge radius, R, and horizontal distance between nozzle exit and model side, S, while keeping the draught, H, constant in part two of his experiment. Except for the values $R/D = 0$ and $R/D = 1.56$ all other parameters are a similar match to the parameter values of the model tests. The propeller slipstream is visualized with adding milk in the slipstream and attaching a long woolen thread in the center of the propeller with the assumption that this would follow the largest velocities in the water, i.e. the centerline of the slipstream. Thon did not measure the results electronically, but extracted his results from photographs during his test runs. The results of Thon's experiment is discussed and compared to the results of the model tests in 9.2.

2.3 Lofterød's experiment

Lofterød (2007) performed an experiment in relation to a master's thesis in 2007 with the title "Coanda-Effect of Azimuthing Thrusters beneath a Hull". The experiment was performed in MARINTEK's Towing Tank no. III, a larger facility than the two prior experiment facilities allowing a larger scale model and presumably less scale effects. The parameters investigated was:

- Thruster diameter $D_{Lofteroed} = 150$ mm
- Variation of Vertical Position of the Thruster, L/D
- Variation of Horizontal Position of the Thruster, S/D
- Variation of Thrust force, T
- Variation of Bilge Radius, R/D
- Variation of Draught, H/D
- Variation of Ship Side Bending, $\alpha_{Lofteroed}$

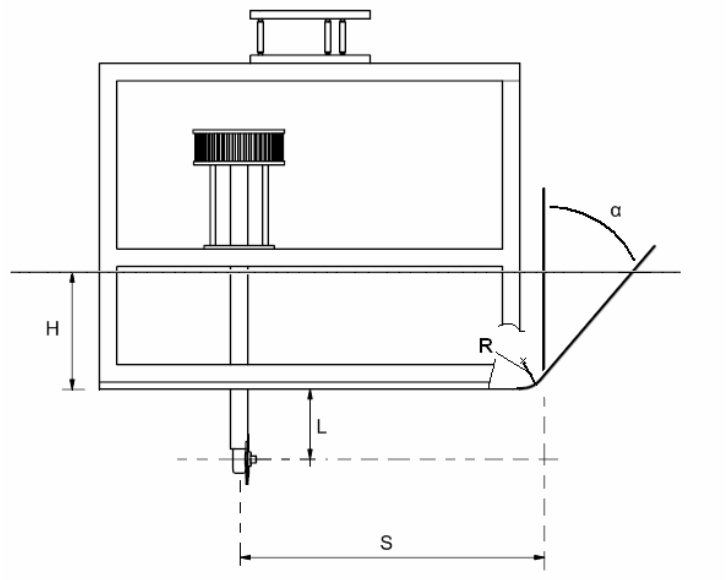

Figure 2.3: Sketch of Lofterød's model with symbols

In 2.3 the model setup with parameter symbols are shown. Lofterød's experiment is also described in 9.1 and in the project thesis, Fjørtoft, prior to this master's thesis. As opposed to the model tests Lofterød did not have a ducted propeller in his experiment. Two force transducers measured the total force on the model and the force on the propeller. In addition video was captured, with threads glued to the model and on a pole downstream of the model to aid the visualization of the slipstream. The range of Lofterøds investigated parameters is shown 2.4. As seen Lofterød did not run all conditions with all variations due to little difference in geometry and thus, in measured results.

R/D [-]	H/D [-]	S/D [-]	L/D [-]	α [°]
0	0.67	2.53	0.83 - 1.17 - 1.5	-
		4.67	0.83 - 1.17 - 1.5	-
		7.00	0.7 - 0.83 - 1.17 - 1.5	-
	1.87	2.53	0.83 - 1.17 - 1.5	-
		4.67	0.83 - 1.17 - 1.5	-
		7.00	0.7 - 0.83 - 1.17 - 1.5	-
0.50	0.67	2.53	0.83 - 1.17 - 1.5	-
		4.67	0.83 - 1.17 - 1.5	-
		7.00	0.7 - 0.83 - 1.17 - 1.5	-
	1.87	2.53	0.83 - 1.17 - 1.5	0 - 14.6 - 28.6 - 36.8
		4.67	0.83 - 1.17 - 1.5	0 - 14.6 - 28.6 - 36.8
		7.00	0.7 - 0.83 - 1.17 - 1.5	0 - 14.6 - 28.6 - 36.8
0.87	0.67	2.53	0.83 - 1.17 - 1.5	-
		4.67	0.83 - 1.17 - 1.5	-
		7.00	0.7 - 0.83 - 1.17 - 1.5	-
	1.87	2.53	0.83 - 1.17 - 1.5	0 - 14.6 - 28.6 - 36.8
		4.67	0.83 - 1.17 - 1.5	0 - 14.6 - 28.6 - 36.8
		7.00	0.7 - 0.83 - 1.17 - 1.5	0 - 14.6 - 28.6 - 36.8

Figure 2.4: Lofterød's test setup and conditions

Chapter 3

Theory on Coanda Effect

There are several mathematical approaches when trying to explain and predict the Coanda effect. The complex nature of a turbulent flow makes a full mathematical and computational solution difficult to obtain and up to now this has not yet been achieved. Through simplifications and assumptions, however, it is possible to derive solutions mathematically which to various degrees fit with reality. This chapter will deal with one mathematical method predicting the attachment length of the slipstream, which would give a good indication of when, and under which conditions, to expect significant thrust losses. Mathematical methods not described in detail in this chapter includes Brix (1993) and Thon (1986).

Brix has derived relatively simple method for predicting the thrust deduction due to Coanda losses. The method is based on dividing the thrust losses into a primary and secondary thrust deduction ratios, where the primary thrust deduction ratio deals with the deflection and the secondary thrust deduction ratio deals with the corresponding increased skin friction. Brix' mathematical method can be found briefly summarized in D.1. Thon has derived a somewhat more complex method to calculate the position of attachment as well as the path of the maximum axial velocity found in the slipstream, u_m, which equals the path of the slipstream centerline. Thon's mathematical method can also be found briefly summarized in 9.2 and 9.3.3.

3.1 Basic theory

When a jet or thruster slipstream passes in the vicinity of a nearby surface it is drawn towards the surface. The closer the jet is to the surface the larger is the attraction force. This is called the Coanda effect.

An central topic in understanding the attraction force acting on the jet is entrainment. In short terms entrainment is the effect that the jet stream attracts fluid from the surroundings and thus adding fluid to the jet stream due to that the jet momentum is preserved throughout the jet. In C.3 the entrainment is derived mathematically, including 3.1 and 3.3 below. This derivation is found in Lehn (1985) and also presented in the project thesis prior to this master's thesis. In short terms the axial momentum must be preserved and thus, with decreasing maximum axial velocity downstream of the thruster the volume flow, Q, must increase with increasing x. Through Prandtl's mixing length theorem this is possible to derive, and the result as shown in 3.3. Entrainment is also described by Rajaratnam (1976).

Lehn (1985) states that:

$$u_m \propto \frac{1}{x} \tag{3.1}$$

$$b \propto x \tag{3.2}$$

$$Q \propto x \tag{3.3}$$

The surrounding water is free to flow from one side towards the low pressure region of the jet except for the side of the jet where a nearby wall is located. While the low pressure can to some extent be relieved on the free side of the jet this is not the case on the "wall side", and thus a transverse pressure distribution would be set up pushing the jet towards the wall, according to Sobey (2000). Faltinsen also states that as the Q increases with x, as shown in 3.3, and as the velocity increases the pressure decreases and consequently a pressure difference across the jet with a resultant force towards the wall is created, according to Faltinsen (1990). The behavior of the axial velocity distribution for a free jet is shown in 3.1.

The jet has a potential core with undiminished axial velocity u_0 from the outlet to a certain point, in 3.1 drawn as a broken line. According to Faltinsen (1990) it takes about six times the thruster diameter before a propeller slipstream develops into a turbulent jet-like flow. Up to this point the flow is regarded to be in a transient phase, and from this point the propeller slipstream is defined as fully developed turbulent flow. After the flow has fully developed the axial velocity distribution takes on a characteristic bell shaped form with a maximum velocity, u_m, in the center, which is decreasing downstream. According to Thon (1986) the rate of entrainment is increasing downstream throughout the transient phase and is fairly constant from the fully developed flow region on.

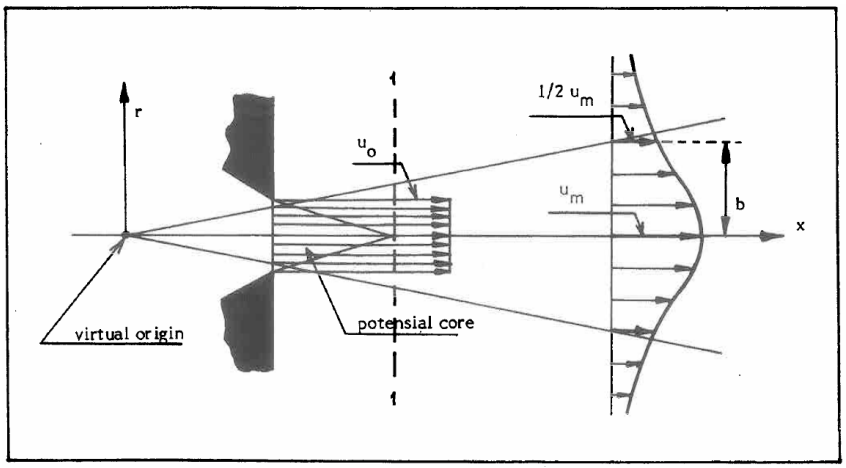

Figure 3.1: Sketch of the axial velocity distribution in a free jet

The bell shaped axial velocity distribution raises the question how to define the spreading angle of the jet. A widely used definition is to define a radial distance $b = \frac{1}{2}u_m$, which is half the maximum axial velocity in the velocity distribution, as a measure of the extents of the jet. According to Faltinsen the jet will spread with approximately 5° using this definition.

The deflection of the jet is throughout the slipstream governed by a force balance between the attraction force and the centrifugal force of the jet, with the attraction force drawing the jet

towards the surface and the centrifugal force drawing the jet radially outwards from the jet center. This is also explained in 3.2, which is collected from Thon (1986). A similar sketch D.1, an explanatory sketch in Brix' mathematical method, also shows this force equilibrium and the suction pressure.

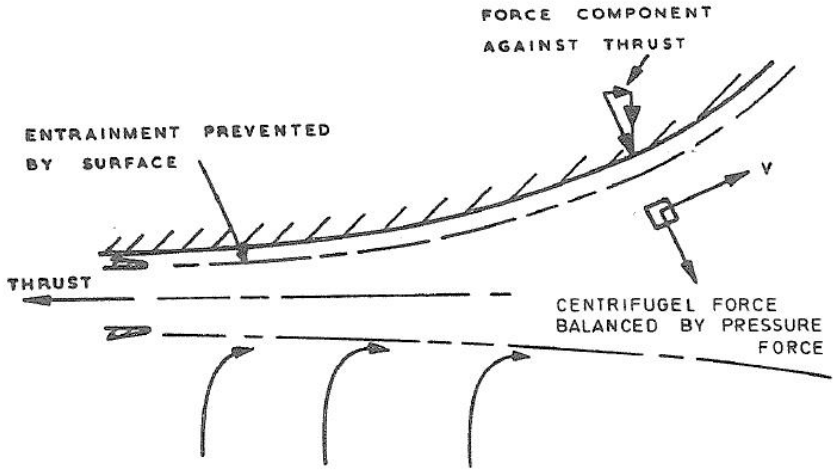

Figure 3.2: Deflection of thruster slipstream

The force balance is central in the mathematical method of Faltinsen, which is the mathematical method focused on in this master's thesis. This mathematical method is not published and will only be a guidance to find mathematical solutions. It is stressed, however, that the method is not the sole work of the author. The method is more thoroughly described in 3.2.

Faltinsen (1990) states that when the slipstream clings to the hull it behaves very much like a wall jet. Whether a wall jet attaches, detaches or reattaches to a wall depends heavily on the geometry of the wall, i.e. the local radius of curvature of the hull. In Köster and Löhr (1964), also referred to in Fernholz (1971), an experimental study on wall jets have been performed, see 3.3. This study includes an investigation of the upper and lower limits of curvature radii to whether a jet will attach to the curvature or not. The experiments show that the lower limit of for the jet to attach to a curved surface is $\frac{R_{geo}}{h} \approx 3$, so that for values of $\frac{R_{geo}}{h}$ lower than 3 the the jet does not adhere to the curved wall. This result is found under the conditions $\frac{l}{h} = \frac{t}{h} = \alpha_1 = 0$. Here, R is the radius of the curved surface, h is the diameter of the nozzle outlet, α_1 is the initial angle of the curved surface, and l and t are the horizontal and vertical distance from nozzle outlet to the curved surface respectively. The variables are described in 3.3, and the denoted symbols used in this subsection are only valid in this example alone, not to be confused with the denotation used in the rest of this master's thesis.

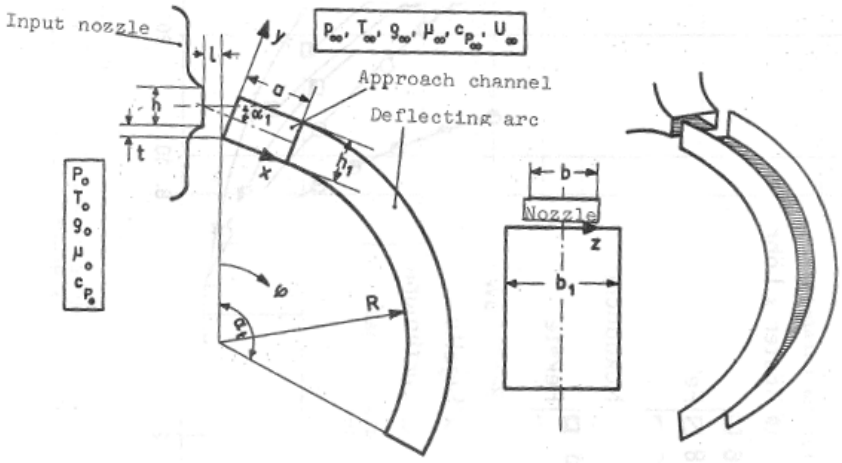

Figure 3.3: Explanatory sketch of Köster's wall jet setup

3.2 Faltinsen's mathematical model

There are, as previously mentioned, several ways of predicting the Coanda effect mathematically. In this section a mathematical method derived by Faltinsen is to be thoroughly described and mathematical results are to be used for comparison with the experimental data in 9.3. The mathematical method predicts the course of the propeller race based on an equilibrium of forces and solved numerically in Matlab. The Matlab source code can be found in the attached DVD. All figures presented in this section is collected from Faltinsen.

The problem description is visualized in 3.4, which also contain the basic parameters in the mathematical solution. The problem setup is a thruster with a possible nozzle tilting α placed a distance a from the hull bottom (in 3.4 drawn as a solid wall). The radius, r_0 of the jet stream is increasing downstream due to the natural spreading of the jet, and the distance h from the solid wall to the jet centerline is decreasing downstream due to the Coanda effect. s is the distance from the jet outlet in the axial direction along the jet centerline. D is the diameter of the nozzle outlet, or the thruster, and s_0 is the distance from the nozzle outlet to the virtual origin of the jet. The virtual origin is described more thoroughly and determined in C.2.

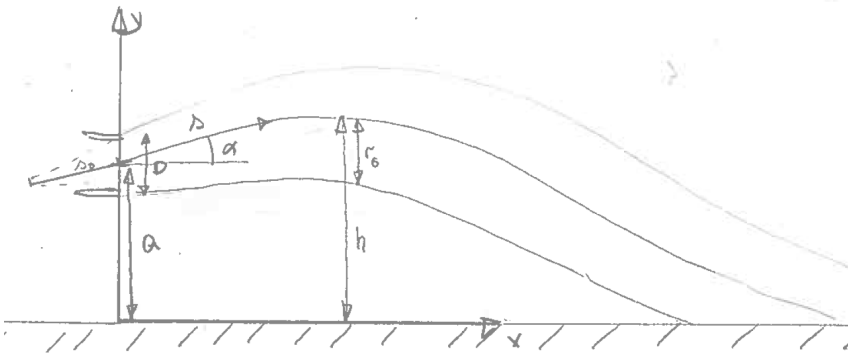

Figure 3.4: Problem description and definition of parameters and variables

3.2.1 Theoretical work

For the numerical solution ds, the incremental change in the value s, will represent each step the force balance has to be satisfied for. The force balance, as previously mentioned, consist of the attraction force between the jet and wall and the centrifugal force of the jet. The force balance initially is defined in 3.4:

$$F_{attraction} = \frac{\rho K}{R}(\text{Centrifugal force}) \tag{3.4}$$

Here, $F_{centrifugal} = \frac{\rho K}{R}$ represents the centrifugal force, which consists of the constant kinematic momentum K, the density of the fluid ρ and the local radius of the gradually more curved centerline of the jet, R, not to be confused with the geometric radius R_{geo} in 3.1. To approach the attraction force a cross section of the jet will be analyzed, see 3.5. Note that this figure has a different coordinate system than 3.4.

As seen in 3.5 the problem description is similar to a sink - source problem, and potential theory can be used to obtain a solution. The sink is located off the x-axis, which is acting as the solid

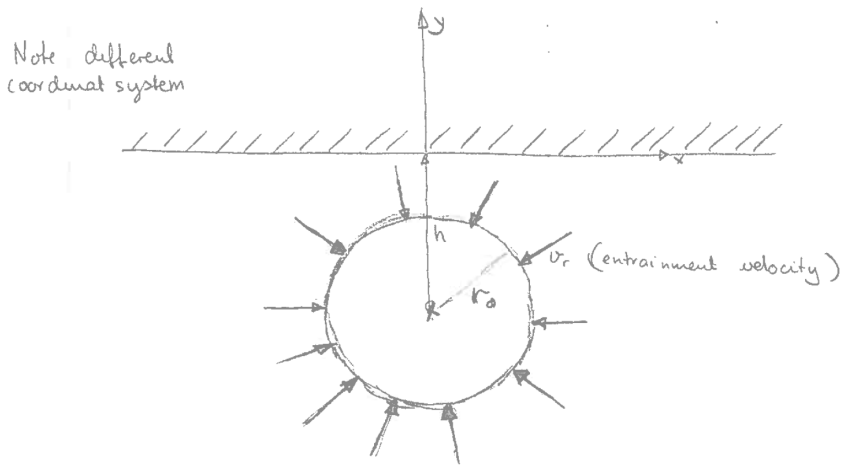

Figure 3.5: Cross section of the jet

wall. To simulate the solid wall a mirror source of equal strength on the opposite side of the x-axis is introduced and thus creating a streamline along the x-axis. The complex solution is obtained from Lamb (1932):

$$w = C \cdot \log\left[(z - ia) \cdot (z + ia)\right] \tag{3.5}$$

where a is the distance between the x-axis (and the simulated solid wall), C is the strength of both sinks and v_r is the positive sink velocity:

$$a^2 = h^2 - r_0^2 \tag{3.6}$$

$$C = -\frac{r_0}{2} v_r \tag{3.7}$$

So far, a complex solution has been obtained in 3.5. To find the forces acting on the jet Blasius theorem can be applied. Blasius theorem can be found in Kundu and Cohen (2002), and states:

$$\mathbb{F} = \mathbb{X} - i\mathbb{Y} = \frac{1}{2} i\rho \oint \left(\frac{\mathrm{d}w}{\mathrm{d}z}\right)^2 \mathrm{d}z \tag{3.8}$$

where $\oint$ is the integral over the whole contour of the body. Blasius theorem applies for any 2-dimensional body contour, which the cross section of the jet in 3.5 can be thought of as. $\mathbb{F}$ represents forces acting on the cross section of the jet, while $\mathbb{X}$ and $\mathbb{Y}$ represents the forces in x-direction and y-direction respectively. The real part of the force acting in y-direction, $\mathbb{Y}$, is of special interest due to it representing the force pushing the jet towards the solid wall. Calculation of 3.8 gives:

$$\frac{\mathrm{d}w}{\mathrm{d}z} = \left(\frac{C}{z-ia} + \frac{C}{z+ia}\right) \tag{3.9}$$

$$\mathbb{F} = \frac{i\rho}{2}\oint_c [\frac{C}{z-ia} + \frac{C}{z+ia}]^2 \,\mathrm{d}z \tag{3.10}$$

$$= \frac{i\rho}{2}C^2 \oint_c [\frac{1}{(z-ia)^2} + \frac{1}{(z+ia)^2} + \frac{2}{(z-ia)(z+ia)}]^2 \,\mathrm{d}z \tag{3.11}$$

$$= i\rho \cdot \frac{C^2}{2} \cdot 2\pi i \cdot \frac{2}{2ia} = \frac{i\rho C^2 \pi}{a} \tag{3.12}$$

where a is negative. Inserting a from 3.7 yields:

$$\mathbb{F} = \mathbb{X} - i\mathbb{Y} = -i\rho \cdot \frac{r_0^2}{4} v_r^2 \cdot \frac{\pi}{\sqrt{h^2 - r_0^2}} \tag{3.13}$$

Extracting the real part of the force pushing the jet towards the solid wall, $\mathbb{Y}$, gives:

$$\mathbb{Y} = F_{attraction} = \rho \cdot \frac{r_0^2}{4} v_r^2 \cdot \frac{\pi}{\sqrt{h^2 - r_0^2}} \tag{3.14}$$

The radial velocity, v_r, remains to be solved. In Schlichting (1968) the axial and radial velocities of an axisymmetric plane turbulent jet are described. It is possible to derive an expression for a axisymmetric circular jet from this, and is derived in C.1. The derived axial and radial velocities of an axisymmetric circular jet is presented in 3.16.

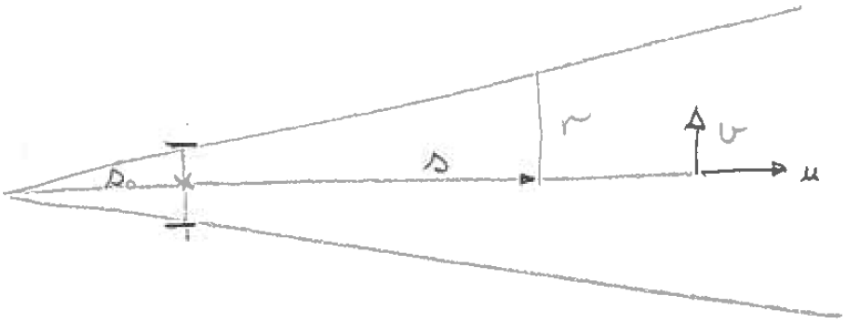

Figure 3.6: Sketch of axisymmetric jet

$$u = \frac{3}{8\pi} \cdot \frac{K}{\epsilon_0 \cdot (s+s_0)} \cdot \frac{1}{(1+\frac{1}{4}\eta^2)^2} \tag{3.15}$$

$$v = \frac{1}{4} \cdot \sqrt{\frac{3}{\pi}} \cdot \frac{\sqrt{K}}{s+s_0} \cdot \frac{\eta - \frac{1}{4}\cdot\eta^3}{(1+\frac{1}{4}\eta^2)^2} \tag{3.16}$$

where η is given by:

$$\eta = A \cdot \frac{r}{s+s_0} \tag{3.17}$$

and A is a constant value given by:

$$A = \frac{1}{4}\sqrt{\frac{3}{\pi}} \cdot \frac{K}{\epsilon_0} \tag{3.18}$$

From 3.17 it is possible to find an expression of r in 3.19.

$$r = \frac{\eta}{A}(s + s_0) \tag{3.19}$$

According to Schlichting (1968) the value is constant and equal to $\frac{K}{\epsilon_0} = 0.0161$. The value of A can then be determined by inserting this into 3.18:

$$A = \frac{1}{4}\sqrt{\frac{3}{\pi}} \cdot 0.0161 = 15.1651 \tag{3.20}$$

η describes the spreading angle of the jet through 3.23. The tolerance limit for the outskirt axial velocities to be regarded as part of the jet, B, is defined in 3.21. As previously mentioned $u = \frac{1}{2}u_m$ corresponding to a $\eta = 1.286$ and a spreading angle of $\beta \approx 5°$ is commonly used, see for instance Lehn (1985). However, to be on the conservative side a $B = 0.1$ is chosen. This corresponds to a $\eta = 2.94$ and a spreading angle of $\beta \approx 11°$, which will result in a decreased attachment length compared to $B = 0.5$.

$$u = B \cdot u_m \tag{3.21}$$

We have that:

$$(1 + \frac{1}{4}\eta^2) = \sqrt{\frac{1}{B}} \tag{3.22}$$

$$\eta = 2 \cdot \sqrt{\sqrt{\frac{1}{B}} - 1} \tag{3.23}$$

Having obtained an expression for the attraction force, $F_{attraction}$, as well as for the radial velocity, v_r, this can now be inserted into the force balance from 3.4:

$$\rho \cdot \frac{r_0^2}{4} v_r^2 \cdot \frac{\pi}{\sqrt{h^2 - r_0^2}} = \frac{\rho K}{R} \tag{3.24}$$

The equation for the force balance, 3.24, now contain the parameters defining the location of the jet stream. It can be numerically solved step by step when knowing the initial values for the variables. Equation 3.24 has been numerically solved through Matlab, with the Matlab source code found in the attached DVD. The theory deduction leading to the Matlab code, however, is given in this subsection.

The desired outcome of solving the force balance is to predict the course of the jet stream and the location of attachment, so consequently 3.24 is solved for with regard to the local radius

of the jet stream curve, R. To simplify the equation the term $r_0 \cdot v_r$ is first analyzed in 3.25. Notice the independence of axial position s.

$$v_r \cdot r_0 = \frac{1}{4} \cdot \sqrt{\frac{3}{\pi}}\sqrt{K} \cdot \frac{\eta - \frac{1}{4} \cdot \eta^3}{(1 + \frac{1}{4}\eta^2)^2} \frac{\eta \cdot (s + s_0)}{(s + s_0) \cdot A} \qquad = \frac{1}{4} \cdot \sqrt{\frac{3}{\pi}} \frac{\sqrt{K}}{A} \cdot \Big(\frac{(\eta - \frac{1}{4} \cdot \eta^3) \cdot \eta}{(1 + \frac{1}{4}\eta^2)^2} \Big) \tag{3.25}$$

Now, reviewing the η, which is given in 3.17 through Schlichting (1968). η contains the information regarding the spreading of the jet and is initially given the value $\eta = 2.94$, meaning that $B = 0.1$, $u = 0.1 \cdot u_m$ from 3.21 and resulting in a spreading angle of approximately 11°. The value of the term inside the parentheses in 3.25 when inserting $\eta = 2.94$ is approximately -1. To make a conservative assumption η is set to draw towards infinity, meaning that $B \to 0$ and physically that the whole radial distribution of axial velocity is included. This will enable predictions of when and where the outer parts of the jet stream first makes contact with the nearby wall. The value of the term inside the parentheses in 3.25 when inserting $\eta \to \infty$ is -4, and 3.25 thus becomes:

$$v_r \cdot r_0 = \frac{1}{4} \cdot \sqrt{\frac{3}{\pi}} \frac{\sqrt{K}}{A} \cdot \Big(-4 \Big) = \sqrt{\frac{3K}{\pi}} \cdot \frac{1}{A} \tag{3.26}$$

Inserting 3.26 into the force balance 3.24 and solving with regard to R yields:

$$\rho \cdot \frac{1}{4} \frac{3K}{\pi} \cdot \frac{1}{A^2} \cdot \frac{\pi}{\sqrt{h^2 - r_0^2}} = \frac{\rho K}{R} \tag{3.27}$$

$$R = \frac{4A^2}{3} \cdot \sqrt{h^2 - r_0^2} \tag{3.28}$$

The deduction of the numerical method used for processing in Matlab can be found in C.4, while the Matlab source code itself is found in the attached DVD. The comparison between the experimental results and the mathematical model can be found in 9.3.

Chapter 4

Model test

The model tests have been performed in close collaboration with MARINTEK. The construction of the model has been done at MARINTEK's workshop.

4.1 Model characteristics

Beside being suited for the investigation of the parameters in the experiment the model characteristics are decided based upon three criteria. First of all, the model should have a general and geometrically simple hull curvature to avoid unknown curvature related flow effects. Secondly, the parameters which are to be investigated should be easy to modify and thirdly, when possible the model should be as similar to Lofterød's model as possible to be able to compare results with the measured data from Lofterøds experiment.

The model consists of four major parts:

- Model hull
- Model frame
- Thruster
- Measurement equipment

The first three are described in this section while the latter is described more thoroughly in 4.2.2.

4.1.1 Model structure characteristics

The model hull is built up of a bottom plate and a side plate made of waterproof plywood, attached together with a bilge made of aluminum and with a radius of 75 mm. Including the bilge radius the total length of the model is 1500 mm and with a breadth of 1200 mm. The model hull is primed and painted to minimize friction losses. The paint color is bright yellow to create a contrast for the underwater camera described in 4.2.2.

The model frame supporting the hull is made of thin walled quadratic aluminum beams with a dimension of $50 * 50$ mm. The exact same frame as in Lofterøds experiment is used, but

somewhat extended due to an increased model length in this recent experiment. The model frame also serves as a foundation for the thruster machinery.

Along the longitudinal center axis there is a slot in the hull bottom for the thruster shaft. After mounting the thruster in one horizontal position the remaining of the slot is sealed with fitted pieces of painted plywood to prevent the opening in the hull to interfere with the propeller race. By sliding pieces of impregnated plywood between the thruster machinery platform and the frame different vertical thruster positions can be evaluated. A more detailed overview of the specific vertical and horizontal positions of the thruster can be found in 5.1. The slots, fitting pieces and thruster machinery with the platform can be seen in 4.2.

4.1.2 Thruster setup characteristics

The thruster machinery is built up of a machinery mounted on a platform resting on the frame, a shaft to a propeller and a nozzle. When the term thruster is used it is meant both the propeller and the nozzle together. The thruster consists of a 4-bladed propeller and a 19A Kort nozzle. Propeller and nozzle characteristics are given in 4.1.

Table generated by Excel2LaTeX from sheet 'B-series'

Table 4.1: Propeller characteristics

Blade number	[−]	Z	4
Pitch ratio	[−]	P/D	1.042
Blade area ratio	[−]	A_e/A_0	0.52
Nozzle diameter	$[mm]$	d_n	190

The thruster is similar to the Wageninger B and Ka4-70 propeller series, although with most similarities to the Wageninger B series. The Wageninger B series is without nozzle, however, as opposed to the Ka4-70. Open water characteristics for the Wageninger B and Ka4-70 series are included in A.4.

4.2 Equipment and facilities

4.2.1 Test facilities

The test basin used in this experiment is the Marine Cybernetics Laboratory, otherwise known as MCLab, located at the Norwegian Marine Technology Research Institute, NTNU. The general test basin dimensions are given in 4.2 and are collected from NTNU.

Table 4.2: Overall dimensions of the test basin, MCLab

Length	40 m
Breadth	6.45 m
Depth	1.5 m

The MCLab is well suited for specialized hydrodynamic tests due to its manageable size and its advanced towing carriage. The relatively short length and breadth of the test basin can, on the other hand, together with the model thruster cause problems with local circulation near

the model. This is further discussed in 8. The towing carriage serves as both the foundation to where the model is anchored as well as the platform of all the measuring equipment. An illustration of the MCLab and the towing carriage, where the model is mounted, is shown in 4.1

The model was installed in the MCLab without water in the test basin. The mounted model with a filled test basin measured surrounding conditions described in 4.3:

Table 4.3: Surrounding conditions in the test basin

Drought of the model	240 mm
Total water depth	1540 mm
Temperature of the water	14°
Density of the water	999.1 kg/m^3
Kinematic viscosity	$1.14 \cdot 10^{-6}$ m^2/s

The density and the kinematic viscosity of fresh water with a temperature of 14 degree is found in ITTC.

Figure 4.1: The MCLab seen from the end of the tank towards the towing carriage

4.2.2 Measuring equipment

Force transducers

The measurements in this experiment are performed with two force transducers. Only forces in x-direction, i.e. the longitudinal direction downstream of the thruster, are measured. The first force transducer measures the total force on the model, F_{tot}, while the second force transducer measures the thrust force from the thruster, F_{prop}. In 4.2 and 4.3 the setup measuring F_{tot} is shown. The location of the force transducer measuring F_{prop} is right beneath the thruster machinery.

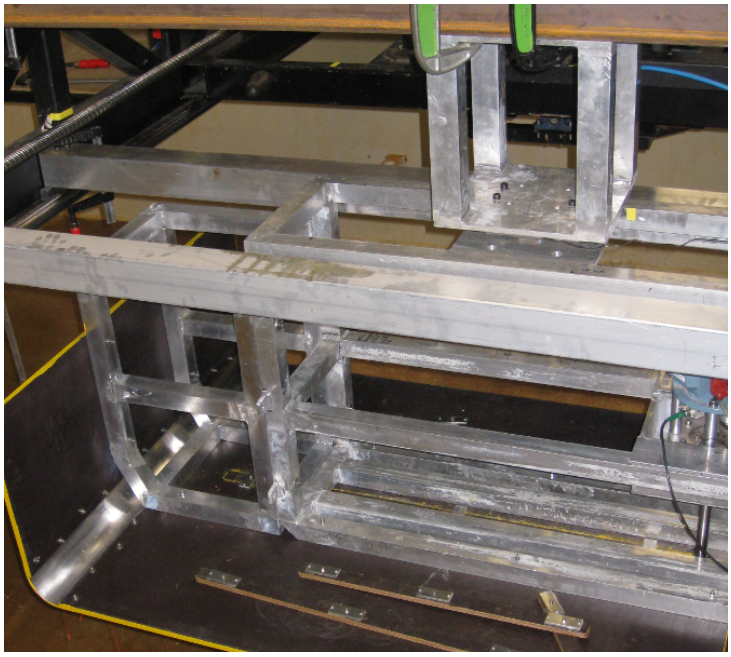

Figure 4.2: Attachment between the model and the force transducer measuring the total force on the model

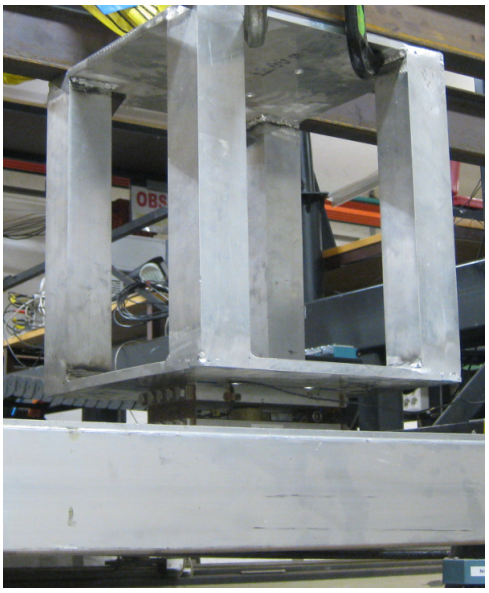

Figure 4.3: Closeup of the force transducer measuring F_{tot}

Data acquisition

For acquisition and time averaging of measured data the computer software Catman is used. The data acquired during the experiment was sampled at a rate of 50 Hz and filtrated at 20 Hz. The time averaged data is inserted into a Microsoft Excel spreadsheet directly from Catman for further analysis. All presentation of measured data in the master's thesis is processed in, and exported from, Microsoft Excel. See the attached CD for the excel worksheet used.

Visualizing effects apparatus

To be able to visualize the direction of the propeller race threads have been glued on to the model. In addition a pole with several threads attached is positioned vertically and 460 mm downstream of the model side to observe the direction of the propeller race after having left the vicinity of the model. The threads are made of nylon, are flexible and have a density slightly larger than the water in the test basin. These properties enable the threads to follow the direction of the surrounding water easily. An underwater camera is used to aid the visual confirmation of the Coanda Effect through video of the model with its glued on threads during the runs. The underwater camera is placed under, and to the side of, the model to include the whole model and the pole with threads in downstream of the model. Video and footage was recorded for each test condition and for all rps within each condition, and can be found in the CD attached to this master's thesis.

The position of the threads are largely based on the experience of Lofterød (2007) from his similar experiment. In 4.4 the position of the attached threads are shown. In addition there are five threads attached on the model side to visualize the potential wake above the bilge. These can be seen in 4.5 along with the other threads attached to the model.

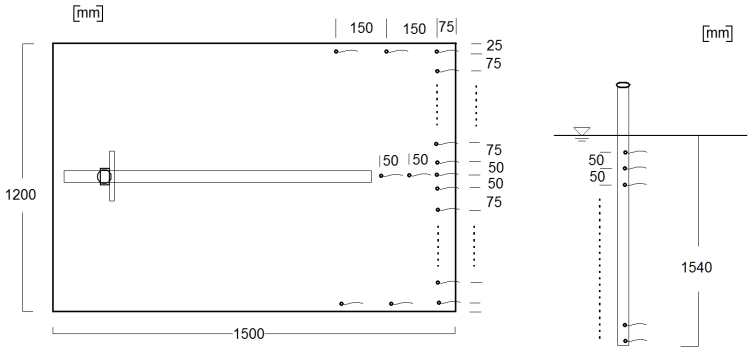

Figure 4.4: Location of the attached threads on the model and pole

4.2.3 Calibration of instruments

Before the MCLab was filled up with water a calibration of instruments took place. The thruster machinery was calibrated with a voltage meter to ensure that the volts applied corresponded with the desired rps, due to the thruster machinery being remote controlled. The two force

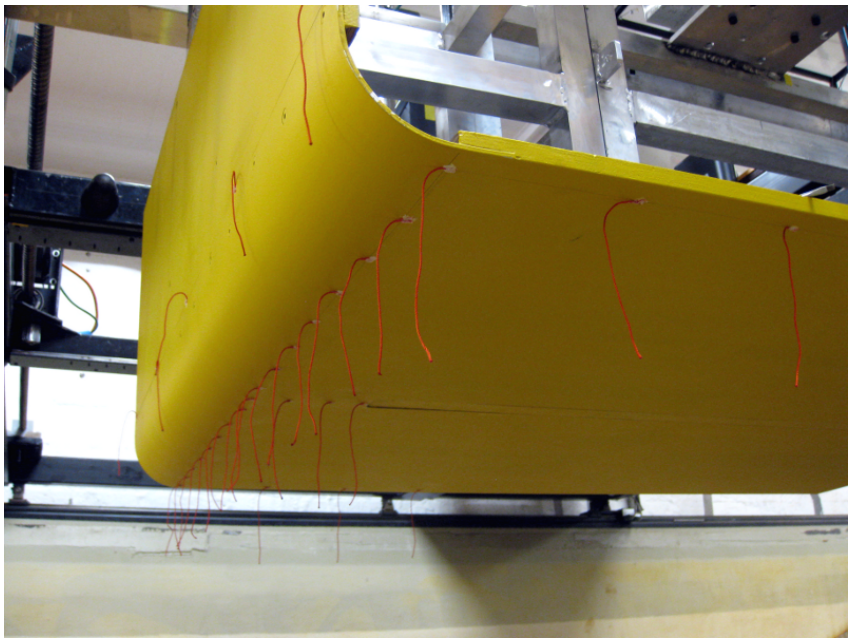

Figure 4.5: Photo of the model with its threads attached

transducers have also been calibrated in advance of the model tests. When changing the geometric parameters between runs there might be additional weight on the model or other changes in the initial measurement values, so a zero measurement has been taken right before the start of each test run to ensure that all measurements start at zero condition.

Chapter 5

Test program

In the lab experiment four different parameters were to be investigated. The construction of the model enabled some parameters to be altered easier than others, which influenced the succeeding order of the parameters. Sorted from the easiest parameter to alter the succeeding order looked like this:

1. Revolutions per second of the thruster
2. Vertical distance from thruster to model bottom
3. Horizontal distance from propeller shaft to the models vertical side
4. Downwards angle of the thruster nozzle

The variations of the parameters were set based on the work of Lofterød (2007) and advice from advisor Sverre Steen. To be able to make comparisons and verifications with the results of Lofterød the variations in revolutions per second, vertical distance from thruster to model bottom and parts of the horizontal distance from thruster to model side were taken directly from his experiment. The increased focus on the variations in the thruster nozzle angle the smallest horizontal distance from propeller to model side was discarded and an equally longer distance was introduced due to the expectation of smaller Coanda effects with thruster nozzle tilting. A longer distance to the model side will, according to the results of Lofterød, cause larger Coanda effects and make the investigation of the effects of the different parameters easier. After advice from Vartdal and Steen the thruster nozzle angles were chosen so to be as authentic as possible to realistic full scale nozzle angles.

The parameter variations are given in 5.1. The values of the vertical and horizontal parameters are made dimensionless by dividing by the propeller diameter, $D = 150\,\text{mm}$, found in 4.1.1. For the parameter vertical distance the three values in 5.1 are the respective distances between the center of the propeller to the model bottom divided by the propeller diameter. For the parameter horizontal distance the three given values are the distances between model side and the center of the propeller shaft divided by the propeller diameter. These parameters are also visualized in 5.1.

There are some routines which are to be followed throughout the test runs. Measurements are to start $5 - 10\,\text{s}$ before the thruster revolutions are increased from zero. During test runs all steps in revolutions, from $10 - 17.5$ rps, are to be measured for approximately 30 s to get an average value within stable conditions. After having reached 17.5 rps the thruster revolutions are to be decreased to 10 rps for a new measurement and further measuring the zero rps condition

Table 5.1: Variations of the parameters

Parameter	Symbol	Unit	Variations			
Revolutions thruster	rps	[rps]	10	12.5	15	17.5
Vertical distance	L/D	[−]	0.70	0.87	1.17	
Horizontal distance	S/D	[−]	4.67	7.00	9.33	
Nozzle angle	α	[°]	0	7.5	10	

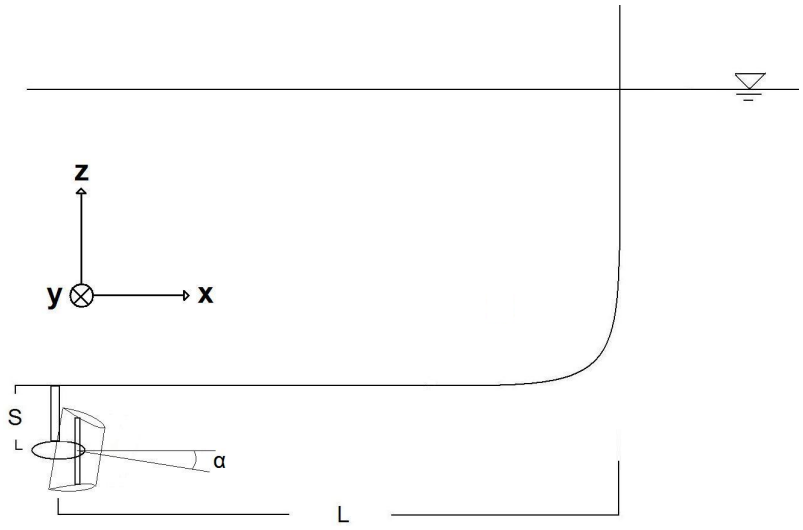

Figure 5.1: Explanation of variation parameters

for $5 - 10$ s before ending measurements of the particular test runs. This is to check whether conditions have changed within each test run.

The test schedule is presented in 5.2 and shows the different test conditions in chronological order. Due to practical reasons the test runs with an nozzle angle of 0° were split into two parts. Also notice that the condition in run no. 21 is equal to run no. 20 due to run no. 21 being a verification run after an overnight pause in the test runs to verify that the premises and surroundings were unaltered. Every fourth run is repeated to verify that conditions have not changed, as also seen in 5.2. 8 deals more with repeated conditions and uncertainties.

Table 5.2: Test schedule for the different conditions

Run no. [–]	Horizontal [–]	Vertical [–]	Nozzle angle [°]
1	9.33	0.7	0
2	9.33	0.87	0
3	9.33	1.17	0
4	9.33	0.7	0
5	9.33	0.7	7.5
6	9.33	0.87	7.5
7	9.33	1.17	7.5
8	9.33	0.7	7.5
9	7.00	0.7	7.5
10	7.00	0.87	7.5
11	7.00	1.17	7.5
12	7.00	0.7	7.5
13	4.67	0.7	7.5
14	4.67	0.87	7.5
15	4.67	1.17	7.5
16	4.67	0.7	7.5
17	7.00	0.7	0
18	7.00	0.87	0
19	7.00	1.17	0
20	7.00	0.7	0
21	7.00	0.7	0
22	4.67	0.7	0
23	4.67	0.87	0
24	4.67	1.17	0
25	4.67	0.7	0
26	9.33	0.7	10
27	9.33	0.87	10
28	9.33	1.17	10
29	9.33	0.7	10
30	7.00	0.7	10
31	7.00	0.87	10
32	7.00	1.17	10
33	7.00	0.7	10
34	4.67	0.7	10
35	4.67	0.87	10
36	4.67	1.17	10
37	4.67	0.7	10

Chapter 6

Test results

In this master's thesis the thrust loss, which is the main subject to be investigated, is evaluated by the use of thrust deduction, t and visual confirmation. The term thrust deduction is described in Minsaas and Steen (2005). The measuring equipment setup described in 4.2.2 allows for a logging of the total force on the model, F_{tot}, the thrust provided by the propeller, F_{prop} , and the corresponding *rps* of the propeller. A formula for the thrust deduction is given in 6.1.

$$t = \frac{F_{prop} - F_{tot}}{F_{prop}} \tag{6.1}$$

As seen in 6.1 the thrust deduction, t, represents the loss of thrust in the system. This thrust loss is considered to be caused by friction loss and loss due to Coanda effect. The value $(1 - t)$ will consequently be a measure for the remaining thrust force available and is used for comparing the different test conditions throughout this master's thesis.

6.1 Variation of rps of the thruster

From the results of Lofterød (2007) the variation in rps from $10.0 - 17.5$ rps is not expected to cause significant deviations in $(1-t)$. Whether the flow, or propeller race, is laminar, turbulent or in a transition phase in between is to a certain degree dependent on the Reynolds number 6.2. In 6.1, taken from White (2003), a flow's dependency of Reynolds number is shown.

$$Re = \frac{U \cdot D}{\nu}$$

where the velocity, U, according to Faltinsen (1990) is defined as

$$U = \sqrt{\frac{F_{prop}}{\rho \cdot A_0}} = \sqrt{\frac{F_{prop}}{\rho \cdot \frac{\pi \cdot D}{2}}}$$

Here A_0 is the area of the propeller disc. This leads to:

$$Re = \frac{2}{\nu}\sqrt{\frac{T}{\rho \cdot \pi}} \tag{6.2}$$

Table 6.1: Phases for flows with different Reynolds numbers

Range Re	Flow phase
$10^2 - 10^3$	Laminar flow
$10^3 - 10^4$	Transition phase to turbulent flow
$10^4 - 10^6$	Turbulent flow with moderate Reynolds number dependency
$10^6 \rightarrow$	Fully developed turbulent flow with small Reynolds number dependency

The variation in rps with the corresponding Reynolds numbers all lie within the range of turbulent flow with moderate dependency of Reynolds number, as seen in 6.2. In addition to the Reynolds number the flow is influenced by geometric factors like roughness of the model surface and velocity fluctuations in the inlet, e.g. propeller race.

Table 6.2: Calculated average Reynolds numbers for different rps

rps	F_{prop}	U	Re
10.0	37.0	1.4	185495
12.5	57.5	1.8	231336
15.0	82.7	2.2	277504
17.5	113.5	2.5	324958

In 6.1 the $(1-t)$ is shown for different rps for the presumably most exposed condition for Coanda effects; namely with $S/D = 9.33$ and nozzle angle $\alpha = 0°$. All runs containing these two conditions are included, meaning all three vertical conditions in addition to the first vertical condition repeated. The graphs show some scatter in the results, although clearly supporting the assumption that variations in rps in the given range will not cause any significant change in $(1-t)$.

In 6.2 the presumably least exposed condition for Coanda effect is shown; namely with $S/D = 4.67$ and nozzle angle$\alpha = 10°$. The graphs show the same pattern as the previously described

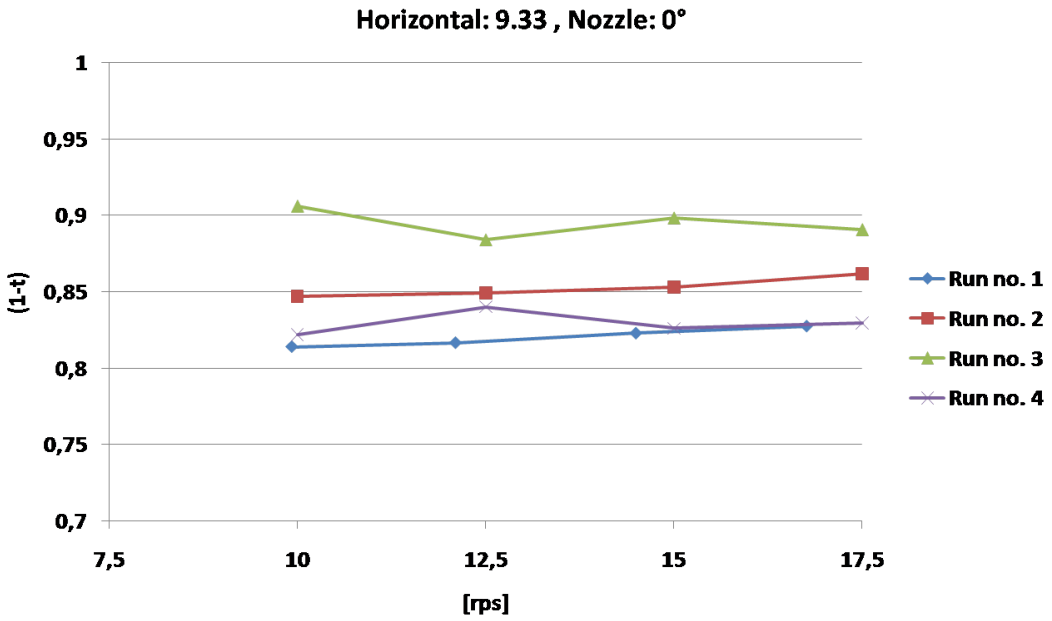

Figure 6.1: Dependency on rps for $S/D = 9.33[-]$ and $\alpha = 0°$

6.1, only with a slightly smaller deviation between the $(1-t)$ of the different runs with their respective vertical variations.

In A.1 additional plots with different horizontal and nozzle conditions are shown. The graphs show the same pattern as 6.1 and 6.2, and further supports the theory that the propeller race measured for each run is less dependent on the Reynolds number and thus, can be described as turbulent flow. It is therefore reasonable to assume that the average $(1-t)$ of all variations in rps within each run can be a good representation of the $(1-t)$ for the respective run. All measurements presented and graphs shown of $(1-t)$ of a run in the following chapters are averaged values of the $(1-t)$ for all rps within the same run.

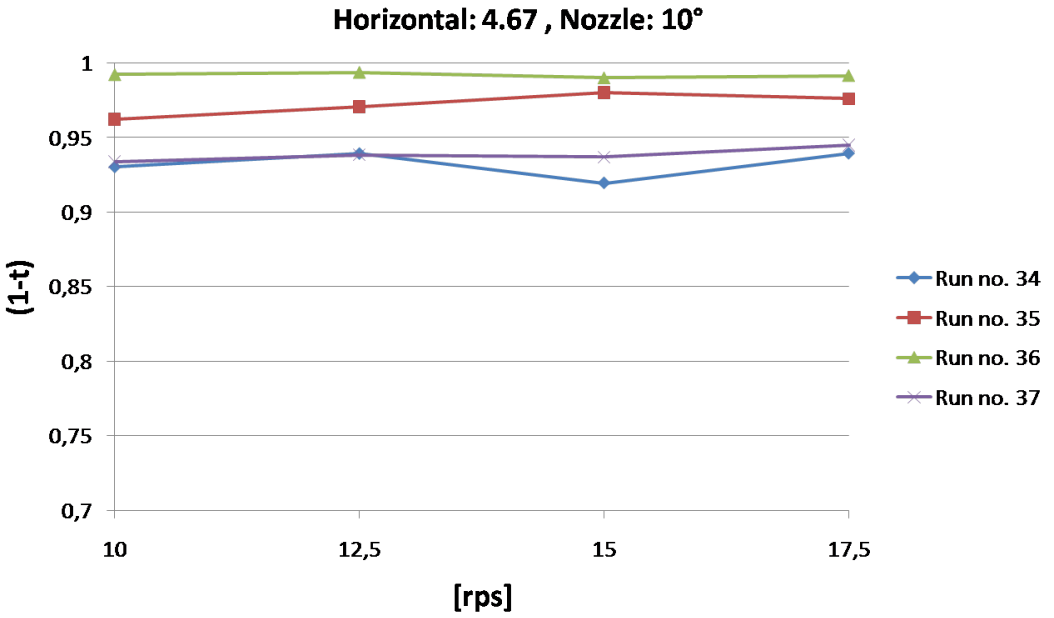

Figure 6.2: Dependency on rps for $S/D = 4.67[-]$ and $\alpha = 10°$

6.2 Variation of vertical position of the thruster

When presenting the effects of varying the vertical thruster position the horizontal thruster position is chosen to be fixed for each figure. The graphs in 6.3 include the $(1-t)$ for all conditions with a horizontal distance $S/D = 9.33$. The following two graphs have fixed horizontal distances of $S/D = 7.00$ and $S/D = 4.67$ respectively.

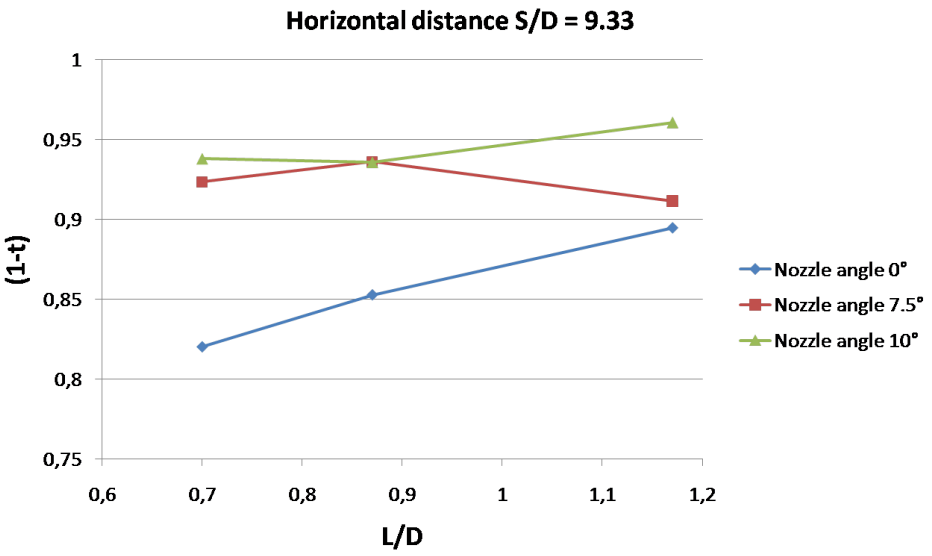

Figure 6.3: Vertical variation with fixed horizontal position $S/D = 9.33$

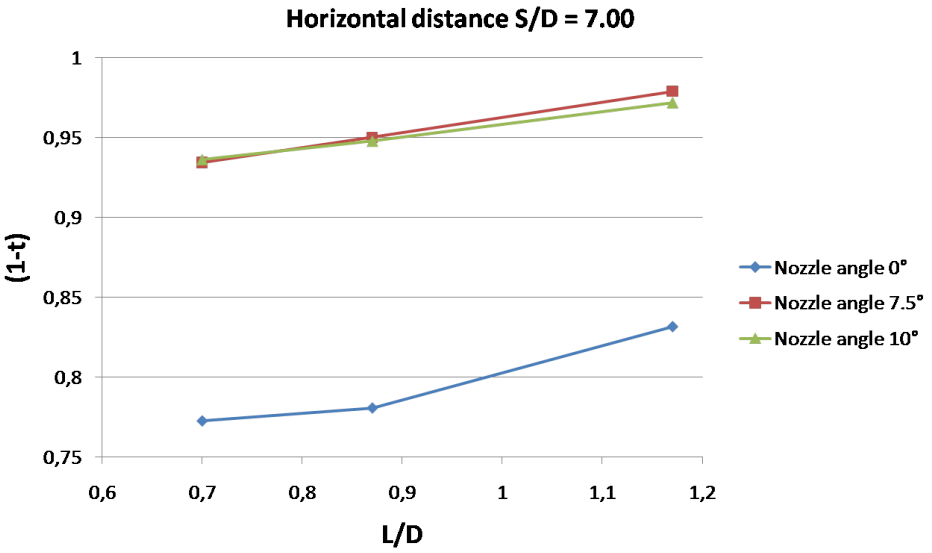

Figure 6.4: Vertical variation with fixed horizontal position $S/D = 7.00$

A horizontal position of $S/D = 9.33$ is presumably the position with most Coanda effect. Surprisingly this is not the case for a nozzle angle of 0°, as can be seen in 6.3 when comparing the 0° graph with the other two figures 6.4 and 6.5. This is commented further in 7.1.3.

The three figures clearly show a trend of increased $(1-t)$ with increasing distance to the model

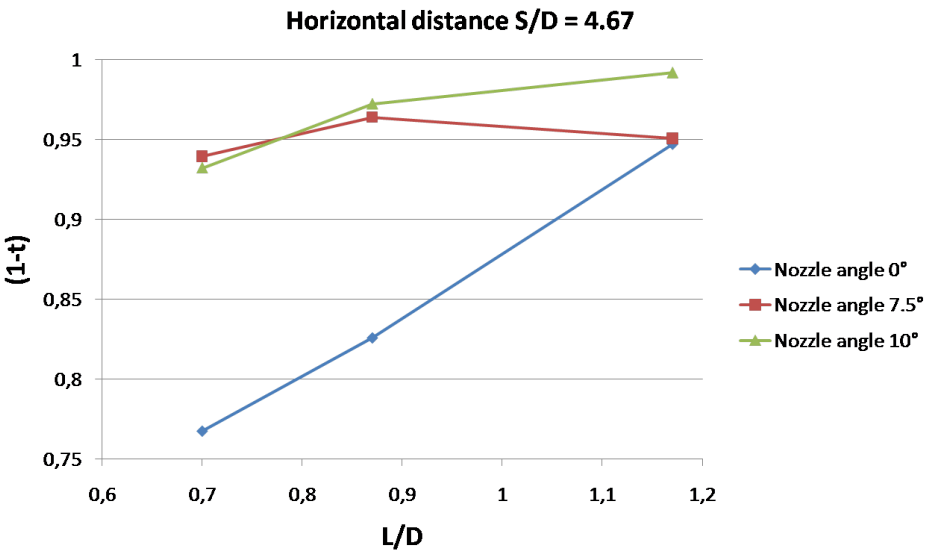

Figure 6.5: Vertical variation with fixed horizontal position $S/D = 4.67$

hull bottom, i.e. larger values of S/D. The graphs with 7.5° and 10° show a generally high value of $(1-t)$ and it is assumed that this is mainly due to the thruster race largely escaping the boundary layer of the model hull. However, since the $(1-t)$ generally increases with increasing L/D even for the least exposed conditions, for instance the combination of $S/D = 4.67$ and $\alpha = 10°$, the thruster race might not have completely escaped the model hull.

An interesting observation is that the thruster race seems to escape the boundary layer close to the model hull for the 0° graph between $L/D = 0.87 - 1.17$ in 6.5. At $S/D = 4.67$ the $(1-t)$ increases very rapidly with increasing L/D for 0°. While the $(1-t)$ for 0° follows the behavior of the other two nozzle angles for the two largest horizontal distances, it increases rapidly to the same order of magnitude for 0° as for the other two nozzle angles with $S/D = 4.67$.

Looking at the same observed phenomenon from 6.8 it is clear that when the thruster is positioned in the shortest distance to the model side the nozzle angle has little to say. It is reasonable to assume that for $S/D = 4.67$ the thruster race escapes the model somewhere between $L/D = 0.87 - 1.17$ regardless of (positive) nozzle angle.

6.3 Variation of horizontal thruster position

To determine the effect of varying the horizontal thruster position the three figures 6.6, 6.7 and 6.8 each have a fixed vertical distance. When following the graph of each nozzle angle one can see the effects on the $(1-t)$ due to horizontal position changes. The model tests have been conducted with three horizontal positions. These decided horizontal positions have been strongly influenced by the work and conclusions of Lofterød. Lofterød concluded to have observed evidence of propeller race adherence in accordance with his mathematical predictions. These mathematical predictions were collected from Faltinsen (1990) and consists of the approximation that a propeller race initially at a distance h from a wall will attach to the wall roughly after $6 \cdot h$. With an additional parameter, namely the nozzle angle, more complex mathematical methods are needed. The results from the model tests should provide evidence of adherence to the model hull in the sense that the $(1-t)$ should suffer a significant drop if this happens.

In addition to measuring the $(1-t)$ several short threads with a transverse orientation have been placed along the center of the model hull to be able to visualize if and where the propeller race adheres to the model hull. Unfortunately the underwater camera resolution was not sufficient to distinguish the transverse threads from the model bottom.

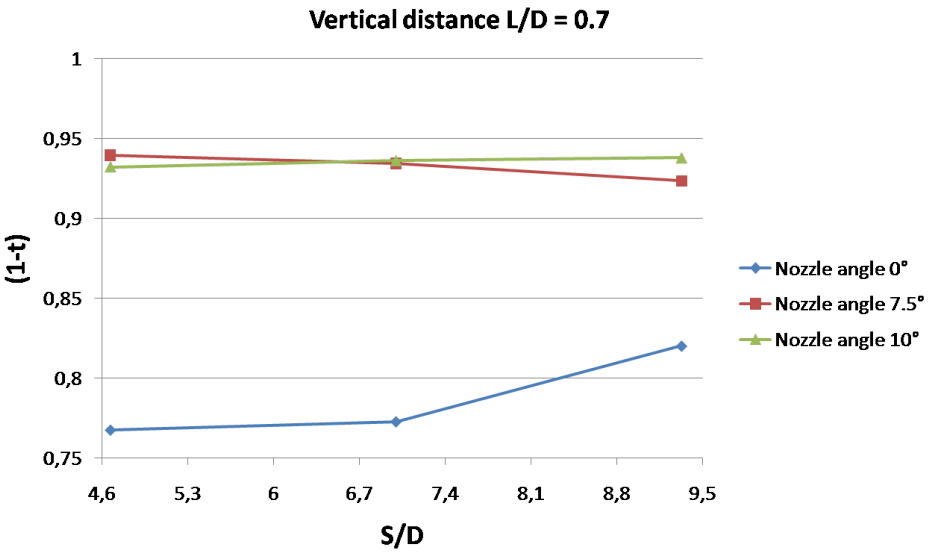

Figure 6.6: Horizontal variation with fixed vertical position $L/D = 0.7$

The results of Lofterød clearly showed a trend of decreasing $(1-t)$ with increasing distance to the bilge and side of the model, and this behavior of $(1-t)$ is expected in the model tests as well. As can be seen in the three figures this is not the case for the graphs with a nozzle angle of $0°$, which has an increased value of $(1-t)$ with increasing value of S/D. This is commented further in 7.1.3.

Figure 6.6, 6.7 and 6.8 all show a decreasing trend of the $(1-t)$ in general when temporary setting aside the values under discussion above. For $\alpha = 7.5°$ and $\alpha = 10°$ the decreasing trend is, however, quite small when considering the extensive geometrical changes when moving the thruster relatively large distances on the model bottom. It is reasonable to assume that the nozzle tilting lets the thruster nozzle escape the model hull to a large degree up to the largest horizontal distance of $S/D = 9.33$. For $\alpha = 0°$ it is difficult to interpret the values of $(1-t)$ in

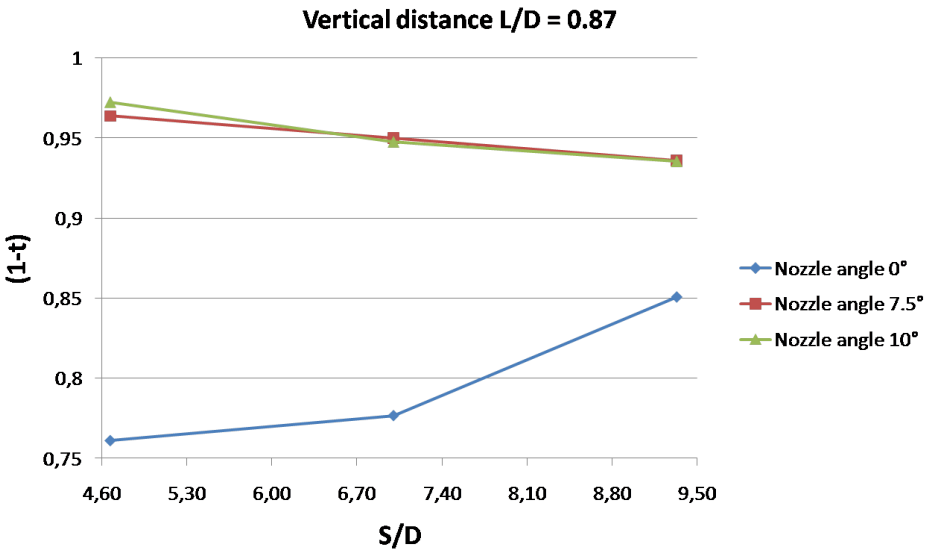

Figure 6.7: Horizontal variation with fixed vertical position $L/D = 0.87$

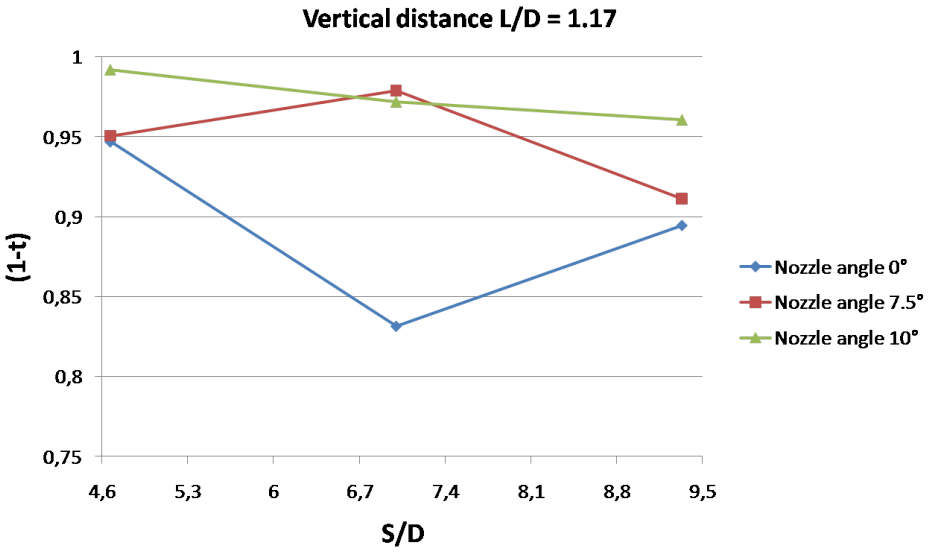

Figure 6.8: Horizontal variation with fixed vertical position $L/D = 1.17$

any direction, due to them being quite contradictory to expected behavior and theory.

When looking closely on 6.9 it is possible to see a change in direction of the pole threads around 600 mm below the surface. This clearly shows that there is entrainment in the vicinity of the propeller race creating a negative velocity from around 600 mm and further down to the tank bottom. Due to a poor contrast color on the pole threads it is difficult to measure a more precise direction of the propeller race, but the bilge threads clearly show that there is a significant upward velocity component present. The data from Run no. 4 indicates the same.

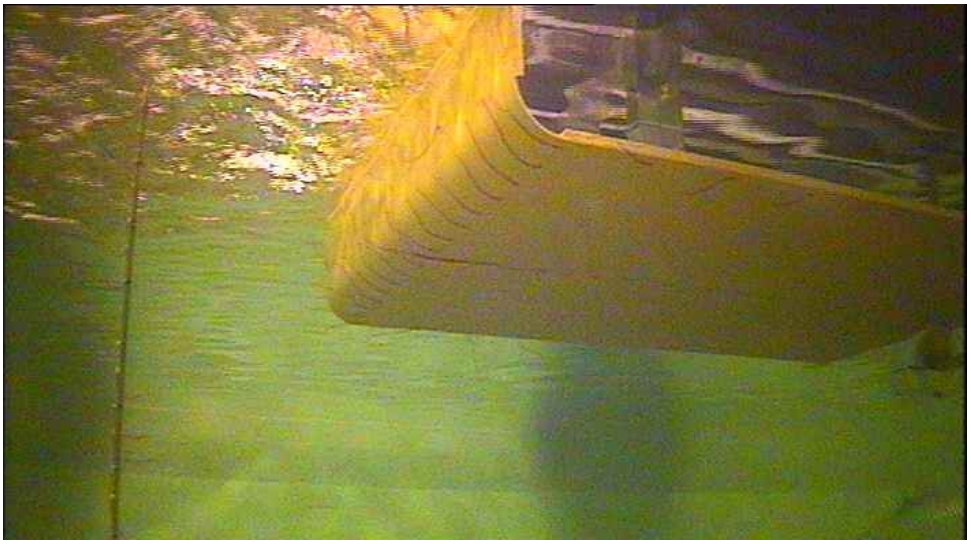

Figure 6.9: Snapshot of Run no. 4 at 17.5 [rps]

6.4 Variation in thruster nozzle angle

The thruster nozzle mounted on the model has three positions, from forward directed in the horizontal plane to 10° downwards tilt. Tilting of the thruster nozzle has traditionally been the preferred precaution to prevent Coanda effect. Investigating of the benefits of nozzle tilting and to which extent this is effective is therefore an important part of the model tests. For the presentation of results in the form of figures the horizontal position has been chosen as fixed for each figure.

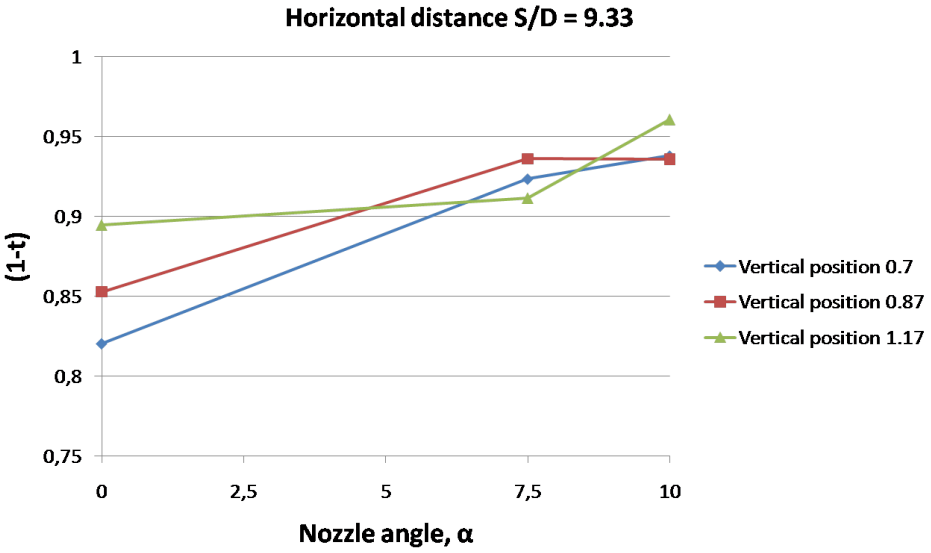

Figure 6.10: Nozzle variation with fixed horizontal position $S/D = 9.33$

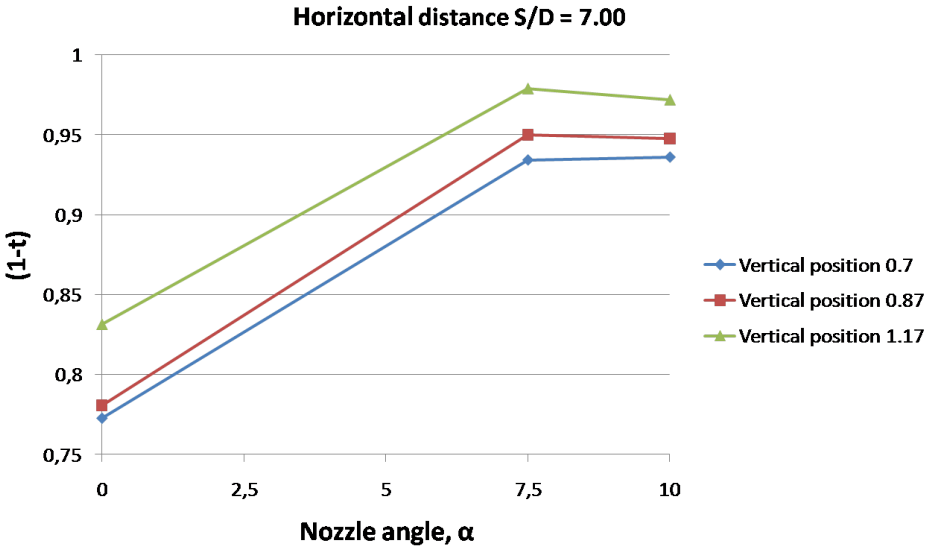

Figure 6.11: Nozzle variation with fixed horizontal position $S/D = 7.00$

When looking at 6.10, 6.11 and 6.12 it is evident that increasing the nozzle angle from $\alpha = 0 - 7.5°$ increases the $(1 - t)$ for all horizontal positions. An interesting observation is that from

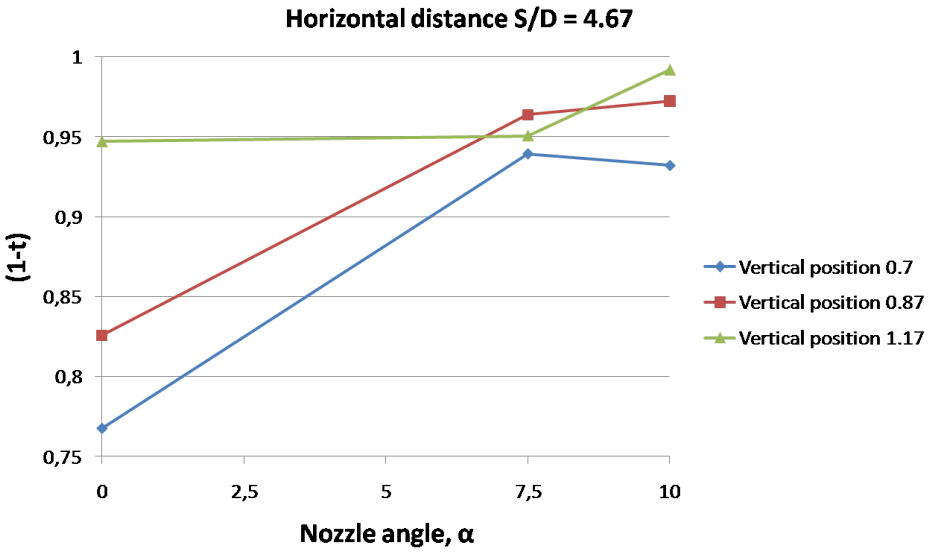

Figure 6.12: Nozzle variation with fixed horizontal position $S/D = 4.67$

$\alpha = 7.5 - 10°$ the $(1-t)$ remains remarkably constant. Consequently, tilting the thruster nozzle more than 7.5° is, according to this observation, not beneficial for increasing the $(1-t)$.

In 6.12 it is quite evident that the condition with $L/D = 1.17$ escapes the model hull regardless of the nozzle angles. The sudden increase in $(1-t)$ for the same graph between $\alpha = 7.5 - 10°$ remains more unclear.However, it is plausible that this is due to the thruster race actually is close to avoiding the model hull completely and thus, the increase in $(1-t)$ is mainly due to reduced friction.

There are some unexpected results within the three figures. One could naturally expect the graph for the vertical position 1.17 to to have a similar shape in 6.10 and 6.11, but is in fact behaving quite differently. Also, the values of $(1-t)$ corresponding to 0° in 6.10 is in general expected to be lower and is discussed in 7.1.3.

Chapter 7

Discussion of test results

7.1 Discussion of measurements

7.1.1 Circulation issues

The test basin with its relatively small dimensions, see 4.3, can increase the chance of local circulation of water around the model and cause an additional force on the force transducers. Continuous observation and extra caution is therefore of the essence during test runs to identify when circulation occurs, stop and let the current fade out before continuing with the runs.

When processing the test results after the model test some results were unexpectedly positive compared to conditions normally less exposed to Coanda effect. After a more thorough examination of the raw data evidence of circulation was found in the force measurements. The routine of starting the measurements $5-10$ s before increasing the thruster revolutions to 10 rps enables an extraction of measured force on the model and the thruster at zero rps and thus, measure any possible force acting in addition to the force supplied into the system by the thruster. All measured data on thruster force and total force used in this master's thesis has been corrected by subtracting any measured initial force. In A.2 the measured initial current force on both force transducers for all test runs are shown. See the attached DVD also for the Matlab script extracting the initial forces from the raw data.

As stated in 5 a measurement with 10 rps has been performed after having reached 17.5 rps in each test run. With this practice there will be two measurements within each test run which, in theory, should be equal and be suitable as a foundation for determining possible changes in the surrounding conditions within each test run. When comparing these two measurements of 10 rps there are large deviations for several test runs. These particular measurements are clearly under the influence of circulation. The measured ending current force is also presented in A.2 and clearly shows the test runs with deviations. This raises the question when the circulation started to influence the results during the test runs, and further directs suspicion to whether for instance the measurements with 17.5 rps are influenced as well. However, after having compared the $(1-t)$ for all revolutions there is little evidence that supports the theory that the measurements with 17.5 rps have been influenced by circulation. The measurements of $(1-t)$ show a fairly constant value, with a slight tendency of increased $(1-t)$ for large revolution numbers, until the final measurements with 10 rps where the values no longer show a uniform pattern. The conclusion is then that correcting for circulation by subtracting the initial forces

in A.2 from the measured values of F_{tot} and F_{prop} is sufficient and that finding a method of subtracting the ending forces as well is not necessary.

7.1.2 Calibration

The experiment setup is largely based on Lofterøds setup in his own experiment. There has been difficulties with retrieving the specific information regarding which propeller Lofterød used in his model, and photographic material has been the main source of information when deciding upon which propeller to use in this experiment. The maximum forces Lofterøds propeller exerted on the force transducers were approximately 75 N and the decision was made to calibrate for forces up to 90 N in this experiment. The maximum forces the force transducers measured in the experiment exceeded the predicted forces, with a maximum of approximately 113 N. This should normally not cause any significant deviations in the measured results, due to the exceeding not being relatively large, but will naturally stand as a potential source of error.

7.1.3 Unexpected values of (1-t)

Test run no. 1-4, with fixed horizontal distance $S/D = 9.33$ and nozzle angle $\alpha = 0°$, show unexpected values of $(1-t)$ compared to other conditions. As seen in 5 these four test runs should, in theory, be the most exposed condition for the Coanda effect and thus have the lowest value of $(1-t)$. However, this is not the case, as the results corresponding to these conditions are approximately (1-t)$= 0.82 - 0.89$, meaning $12-18\%$ thrust loss. This value of $(1-t)$ is quite high, especially when comparing with presumably "better" conditions, for instance the conditions in run no. 17-20, with fixed horizontal distance $S/D = 7.00$ and still a nozzle angle of $\alpha = 0°$. Run no. 17-20 should result in a lower Coanda effect loss due to the shorter distance between thruster and bilge, but results show that (1-t)$= 0.77 - 0.83$ meaning a thrust loss of approximately $17-23\%$. The measurements of local current, described in 7.1.1, show that there is little or no current present during run no. 1-4. There is also very little scatter with varying thrust force in addition to the runs having an expected increased $(1-t)$ when increasing the vertical distance L/D.

A theory that could explain this presumably increased value for run no. 1-4 could be, as suggested in 6, that conditions with shorter distance from thruster to bilge S/D might have a more favorable angle of attack onto and over the bilge resulting in an increased thrust loss compared to conditions with larger S/D where the jet stream has already attached to the hull and has a more violent bilge curve and might detach at an earlier stage, as mentioned in Lehn (1985). However, when looking at run no. 22-25, with the same $\alpha = 0°$ but with an even shorter distance to bilge $S/D = 4.67$, the measurements show that this described phenomenon with favorable angles of attack on the bilge occurs within these last mentioned test runs, also seen clearly in 6.5.

Another theory is that the thruster itself has not been attached properly during run no. 1-4, which might have resulted in the thruster shaft barely touching the model and increasing the forces measured on the model. This could explain the increased $(1-t)$, but the probability that this would happen to all four runs is not very probable. In addition the measurements with different thrust forces within the same run would show a large scatter due to the thruster shaft being pushed increasingly backwards with increasing thrust force applied. This is not evident, and further decreases the probability of this being an explanation for the deviant results. As far as the investigation of the unexpected results from run no. 1-4 goes no plausible explanation

has been found. These results are therefore included as normal in the overall results, although a decision to not draw any conclusions based on these particular results alone has been made.

7.2 Measurements influenced

During the rearranging of parameters in run no. 24 the measurement equipment measuring the rps of the thruster suffered some damage and had to be shut down. The rest of the experiment was carried out with adjusting the thruster rps by inserting the calibrated values of voltage directly in the thruster machinery. The results should not be influenced by this, although the readings of the rps are not included in the experiment results after this run.

The forces measured on the model are strictly in axial direction. However, as can be seen in the video footage on the attached CD there are transverse oscillations during some runs. This is evident for the conditions with $\angle = 0°$ and $L/D = 0.7$ in particular, meaning the conditions where the jet stream is closest to the model bottom. It is possible that these small heave motions may influence the results during measuring. For most conditions this oscillations were not present.

7.3 Validity of experiment

The measurements have been performed on a relatively small model in calm water and with no current present. It is said previously that to experience a thrust loss of up to 25% during a real scale offshore operation in harsh weather conditions would be a very serious situation. However, the results obtained in calm environments during model tests might not be valid for more than a percentage of the working life of for instance a semisubmersible platform or an offshore supply vessel.

The results from the model tests prove that tilting the thruster downwards is a very effective countermeasure against thrust loss due to Coanda effect when the thruster is completely tangential to the ship side, and the loss related to the thruster tilting is small compared to the Coanda loss. Considering a life cycle of an offshore supply vessel however, it is not evident that having a fixed downwards thruster tilt will be the best alternative altogether, due to the Coanda effect not being relevant without certain conditions being met.

It is clear that the deflection of a jet around the bilge resulting in the jet hitting the other pontoon for a semi submersible platform will represent a large thrust loss. However, if a current is present in the vicinity of the jet stream it is not evident what would happen to the jet stream from it leaving the first pontoon and to hitting the other pontoon which could be approximately 50 m in order of magnitude, according to Lehn (1985).

In large waves resulting in large heave and pitch motions there might be many additional parameters influencing the total thrust loss and altering the conditions required for the Coanda effect to have a significant effect. For example ventilation may occur, and the effect on the jet stream with changing draught movement of the source, namely the thruster, may reduce the validity of the results acquired from the model tests.

Chapter 8

Uncertainty analysis

In this uncertainty analysis the focus will be on an error analysis in the form of a 95% confidence interval. A 95% confidence interval is an interval in which the true value of a certain measurement lies with a probability of 0.95. Due to the fact that it is close to impossible to rule out all uncertainties in tank experiments such as this it gives meaning to talk of acceptable uncertainty and intervals in which measurements are expected to lie within. A confidence interval is in this case a very useful tool for evaluating measurement data. The word "error" will in this master's thesis describe the deviation between the true value, which is unknown, and the measured or calculated value for the same case. An error can be caused by a variety of reasons, but common for all is that they can be categorized in two categories; namely "Precision errors" and "Bias errors". The two categories can be combined to find a total error. This whole chapter on uncertainty is largely based on Aarsnes and Steen (2008) and Walpole et al. (2007).

8.1 Precision errors

Precision error can be revealed as scatter in the measurement of repeated runs. A precision error could for instance be a small circulation in the tank at certain runs interfering with the measurement of those specific results. Another example of a precision error could be that the geometry of the model will differ slightly for specific runs as the geometry is altered for different conditions. Common for all precision errors is that the deviation with the true value will decrease with an increased number of repeated runs. A specific run with a large precision error will be less significant for the overall results as the amount of measured runs increases.

The precision error in a measurement, if repeated an infinite number of times, is assumed to follow a Gaussian distribution around a mean. In this experiment the number of repetitions of a certain condition is relatively small and not well suited for establishing an accurate value of the mean. It is, however, possible to estimate the mean with a student's t-distribution which does not necessarily require a large number of repetitions. Looking at the test schedule in 5 the condition with the largest number of repetitions can be found within the run no. 17, 20 and 21, which are identical. As described in 7.1.1 the 10 rps is measured twice within each run. Thus, for the condition with $S/D = 7.00$, $L/D = 0.7$ $\alpha = 0$ degree and 10 rps there are a total of $3 \cdot 2 = 6$ repetitions.

The precision limit for the mean values of the given repetitions can be found with 8.1 and is dependent on the standard deviation, S_x, the weight $t_{0.05}$ of the student's t-distribution and

the number of repetitions, N. The subscript of $t_{0.05}$, related to a 95 % confidence interval, is specified already from the general equations in this section to avoid confusion with the sign for the thrust deduction, t.

$$P_{\overline{x}} = \frac{t \cdot S_x}{\sqrt{N}} \tag{8.1}$$

The standard deviation is defined as:

$$\overline{X} = \frac{1}{N} \sum_{j=1}^{N} X_j \tag{8.2}$$

$$S_x = \sqrt{\frac{1}{N-1} \sum_{j=1}^{N} (X_j - \overline{X})^2} \tag{8.3}$$

where $\overline{X}$ is the mean value. The value of the weight, $t_{0.05}$, of the student's t-distribution can be found in the appendices of Walpole et al. (2007).

8.2 Bias errors

While precision errors can be revealed and identified with an increased number of repetitions, bias errors are a totally different matter. Bias errors are systematic errors and will influence all repetitions. An example of a bias error could be an inaccurate calibration of measurement equipment. When looking at the measurements afterwards all data will have a deviation from the true value, but the error will be impossible to measure due to that the measurement equipment itself contains the error. Common for all bias errors is that an increased number of repeated runs will not result in a smaller error. Prevention of bias errors is largely limited to being aware of all possible bias errors and eliminate as many as possible prior to the experiment. Estimates of the bias error in an experiment will rely heavily on experience and qualified guesses.

Errors in the calibration of measurement equipment has already been mentioned, but there are several possible bias errors that will in various degrees influence the results of this experiment. Due to problems with the spray painting equipment the model was rolled on by hand. It is plausible that this might have resulted in a less smooth model surface and thus an increased friction coefficient of the submerged model surface. Due to that the experiment is not meant to be scaled up and compared directly with real vessels this will not be a significant bias error for this experiment. When comparing with other experiments, for instance with Lofterød's experiment, it is likely that this would cause a constant deviation between the results of both experiments that will not decrease with an increased number of runs.

A tank experiment will in general contain both precision and bias errors. If the results from the model test are to be scaled up and used in full scale calculations the bias error will be important to estimate. In this master's thesis' experiment, however, the results are to be compared and evaluated only within the realm of the tank. The assumption is then that all measurements within this experiment will contain the same bias error and will be less significant for the results acquired. While Lofterød (2007) in his experiment calculated with a bias error of 1% for the measurement of the thruster's thrust, F_{prop}, and 4% for the measurement of the force on the model, F_{tot} the bias error will be disregarded in this uncertainty analysis. The precision error

and the total error will then be equal.

8.3 Error analysis

Performing an error analysis of an experiment is important for validating results. The error analysis method used in this section is listed in itt (1990) and is also found in Aarsnes and Steen (2008).

8.3.1 Reduction equation

A reduction equation is the functional relationship between parameters within the repetitions and is shown in general in 8.4. Here, X is the measured sample and f_r is a function of relevant sample parameters. This reduction equation can, assuming a small change in each Y_i results in a small change in the measured value, be solved through Taylor expansion, see 8.7.

$$X = f_r(Y_1, Y_2, \ldots, Y_N) \tag{8.4}$$

$$X = \hat{X} + \frac{\partial \hat{X}}{\partial Y_i}\Delta Y_i + \frac{1}{2}\frac{\partial^2 \hat{X}}{\partial Y_i^2}\Delta Y_i^2 + O(\Delta Y_i^3) \tag{8.5}$$

$$\simeq \hat{X} + \frac{\partial \hat{X}}{\partial Y_i}\Delta Y_i \tag{8.6}$$

$$= \hat{X} + \kappa_i \cdot \Delta Y_i = \hat{X} + e_i \tag{8.7}$$

where κ_i is the influence coefficient and e_i is the elemental error for each parameter. The absolute value of ΔY_i is unknown but can be estimated with the precision limit, P_i, based on a confidence interval, see 8.8.

$$\Delta Y_i = P_{Y_i} = P_i \tag{8.8}$$

8.3.2 Error propagation

The error propagation is the combined effect on the measured value from all elemental error sources. Assuming that all elemental error sources are independent the precision and bias elemental error can be found by combining all contributions with the root square - sum square method:

$$e_P = \sqrt{\sum_{i=1}^{N} (\kappa_i \cdot P_i)^2} \tag{8.9}$$

$$e_B = \sqrt{\sum_{i=1}^{N} (\kappa_i \cdot B_i)^2} \tag{8.10}$$

The bias error is neglected due to its lesser significance for this experiment. Consequently, the total elemental error, e_T, is equal to the precision elemental error, e_P:

$$e_T = \sqrt{e_P^2 + e_B^2} = e_P \tag{8.11}$$

When $\hat{X}$ is a measurement and e_T is the total error the true value of X is found within:

$$X = \hat{X} \pm e_T \tag{8.12}$$

with a probability of 95 %.

8.3.3 Analysis of the experiment

The measurement samples used in the error analysis is given in 8.1. There are a total of 6 repeated measurements, all taken with 10 rps.

Table 8.1: Three test runs supplying the repetitions for error analysis

Parameter		Run no. 17		Run no. 20		Run no. 21	
	1st	2nd	1st	2nd	1st	2nd	
rps	$[rps]$	10.0074	10.0060	9.9992	.9983	10.0104	10.0071
F_{tot}	[N]	28.0435	28.8017	27.6325	27.8872	27.8908	28.7005
F_{prop}	[N]	36.9105	36.8961	36.7892	36.2548	36.6766	36.4909
$(1-t)$	$[-]$	0.7602	0.7811	0.7394	0.7577	0.7603	0.7863

Relating this to the actual experiment, the parameters Y_1 and Y_2 from 8.7, are identified as F_{tot} and F_{prop} while $\hat{X}$ is the $(1-t)$. Consequently, κ_{tot} and κ_{prop} are defined as:

$$\kappa_{tot} = \frac{\partial(1-t)}{\partial F_{tot}} = \frac{\partial}{\partial F_{tot}} \left(\frac{F_{tot}}{F_{prop}} \right) = \frac{1}{F_{prop}} \tag{8.13}$$

$$\kappa_{prop} = \frac{\partial(1-t)}{\partial F_{prop}} = \frac{\partial}{\partial F_{prop}} \left(\frac{F_{tot}}{F_{prop}} \right) = -\frac{tot}{F_{prop}^2} \tag{8.14}$$

The precision limit can be found with 8.1. The weight $t_{0.05}$ with a corresponding 95 % confidence interval and $N-1=5$ degrees of freedom can be found either in Walpole et al. (2007) or with the built in t-function in Microsoft Excel. The latter has been chosen in this error analysis. Steps and results from the calculation of κ is given in 8.2.

The total precision error given in 8.10. As previously mentioned the bias error is neglected and consequently $e_P = e_T$, as stated in 8.11. In 8.3 the final results are given. In addition the 95 %

Table 8.2: Calculation of precision limit of the mean

Y_i	$\overline{X}$	S_x	N	$t_{0.05}$	P_x	$P_{\overline{x}}$	κ	$\kappa \cdot P_{\overline{x}}$
F_{tot}	27.824	0.899	6	2.571	2.310	0.943	0.027	0.026
F_{prop}	36.406	0.551	6	2.571	1.416	0.578	-0.021	-0.012

confidence interval, with reference to 8.12, for the mean value of $(1-t)$ is given.

Table 8.3: Results from the error analysis

$(1-t)_{mean}$	e_{tot}	$(1-t)-e$	$(1-t)+e$
0.764	0.029	0.736	0.793

As seen in 8.3 the calculated total error for run no. 17, 20 and 21 are $e_{tot} = 0.029$. With an increased number of identical runs e_{tot} would probably be reduced, according to Aarsnes and Steen (2008), but with only six identical runs the error is quite sensitive for scatter in the results. The total error calculated is therefore regarded as a conservative estimate of the total error and is regarded as valid for any test run in this experiment. A 95 % confidence interval for the $(1-t)$ for any test run can therefore be established by establishing an upper limit by adding e_{tot} to the measured value and subtracting e_{tot} from the measured value for establishing a lower limit, as done for the specified mean value of $(1-t)$ in 8.3.

Chapter 9

Implementation and comparison

To verify results it is utmost important to compare results with other sources. The results from the model tests performed in relation with this master's thesis can to some extent be compared with the similar experiment of Lofterød (2007). In addition the results can also to some extent be compared with a mathematical model from Faltinsen for the benefit of both the model test results and the validity of the mathematical predictions.

Naturally there are challenges related to comparing results with difference in e.g. time, environment, equipment and the human work methods even when the parameters investigated are the same. The four parameters investigated in this master's thesis' model tests are:

- Variation of vertical position of the thruster
- Variation of horizontal position of the thruster
- Variation of thrust force
- Variation of nozzle angle

The variation of thrust force is counted as a parameter for both the model tests and Lofterøds experiment, although not always treated as a full parameter in the master's thesis due to it not being a geometrical parameter and that there is little difference in $(1-t)$ for different thrust forces.

9.1 Comparison with Lofterøds experiment

The model tests are initially based upon Lofterøds experiment, although there are some planned and unplanned differences. Lofterøds experiment consisted of these six parameters:

1. Variation of Vertical Position of the Thruster
2. Variation of Horizontal Position of the Thruster
3. Variation of Thrust force
4. Variation of Bilge Radius
5. Variation of Draught
6. Variation of Ship Side Bending

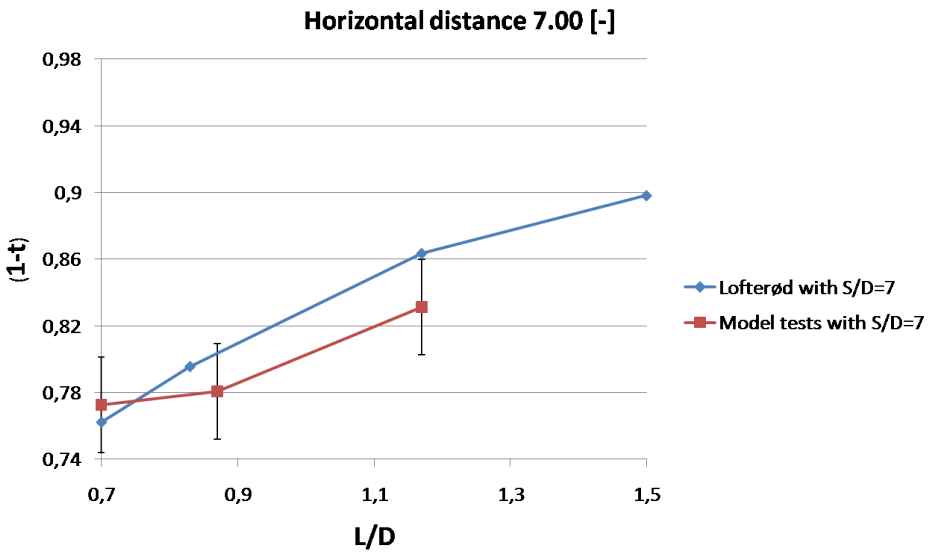

Figure 9.1: Comparison with Lofterød, fixed horizontal position $S/D = 7.00$

Parameters no. 1 to 3 are equal for both the model tests and Lofterøds experiment, while one of the settings in each of the other parameters in Lofterøds experiment are a fixed value in the model tests. For instance, Lofterød has investigated four settings of ship side bending, namely 0°, 14.6°, 28.6° and 36.8°, while in the model tests the orientation of the ship side is fixed to 0°. This parameter alone eliminates many of the test runs from Lofterøds experiment from the comparison.

The variation of bilge radius and draught showed significant differences in $(1-t)$ in Lofterøds results, and settings other than bilge radius $R/D = 0.5$ and draught $H/D = 1.73$ are discarded for comparison. The ship side bending showed that there was little difference in the two smallest angles, namely 0°, 14.6°, and may both be used. However, these two settings are redundant and only 0° is therefore needed for comparison. A compromise is made when combining both the need for overlapping data with Lofterøds experiment as well as the motivation for taking the investigation of the parameters further. For parameter no. 1 and 2 two out of the three settings from Lofterøds experiment are kept while one is discarded and replaced with a new setting. The rps of both model tests and Lofterøds experiment are identical, although the advance coefficient is different and produces different thrust forces. See 7.1.2 for more details on this matter.

After a review of identical parameters a total of five runs are similar and an additional five supplementing runs with one variation outside the variation in the model tests. The comparison is divided into four figures; 9.1 and 9.2 compares the two similar settings in the variation of horizontal thruster position, while 9.3 and 9.4 compares the two similar settings in the variation of vertical thruster position. The supplementary runs provide extensions of the graphs and is, in that way, useful for the comparison.

In 9.1 and 9.2 a comparison with fixed horizontal position is done. If the model tests and Lofterøds experiment have been set up and carried out in the same fashion only a difference in friction should be the source of any difference in the results. The difference in friction should cause a fixed difference in the results as can be seen in 9.1. While 9.1 shows a behavior with relatively equal difference quotient the situation is somewhat different for 9.2. As can be seen in 9.3 as well, the results disturbing the expected equal behavior is found in the run with

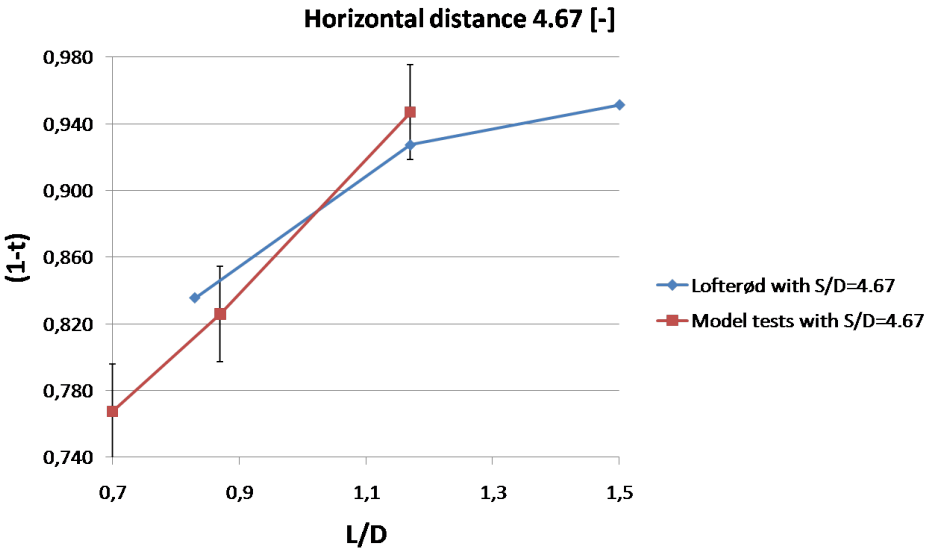

Figure 9.2: Comparison with Lofterød, fixed horizontal position $S/D = 4.67$

$S/D = 4.67$ and $L/D = 1.17$. In 9.4 the equality in the difference quotient can be seen for the $(1-t)$ related to the similar runs. The last reading in the graphs of the model tests in 9.3 and 9.4 leaves a positive trend in $(1-t)$, which is not as expected. This is discussed previously in 7.1.3.

When evaluating the comparison with Lofterøds experiment the results in general show a similar behavior, although run no. 24 in the model tests disrupts this pattern. Friction is thought to be the significant source of difference in the $(1-t)$. Lofterøds model did not, however, have a nozzle on the propeller, and this could be another source of difference in $(1-t)$.

9.2 Comparison with Thon and Lehn

Thon (1986) and Lehn (1985) have performed similar experiments in 1986 and 1985 respectively, and is described more thoroughly in 2, and in the project thesis, Fjørtoft, prior to this master's thesis in addition. Thon performed his experiment "Deflection of propeller slipstream" with a smaller model and propeller, and a Reynolds number for the propeller race of $Re = 10.7 \cdot 10^4$. According to Thon the entrainment rate is found to be independent of Reynolds number when $Re > 4 \cdot 10^4$ and thus, should be suited for comparison with model tests of different geometric size.

In 9.5 the comparison with part two of Thons experiment, Lehns results and the model tests are made. The figure is collected from Thon (1986) and is further processed to include the results from the model tests. The figure includes the results of Lehn, with the graph marked with "/3/" in the figure legend.

It is difficult to compare the results of the model tests with these results of Thon and Lehn due to different parameter settings. The large difference in draught, H/D, especially raises doubt to the validity of the comparison. Lofterød investigated two settings of the draught, $H/D = 0.67$ and $H/D = 1.73$, and discovered a reduction in $(1-t)$, and consequently an increase in the thrust deduction t, with increasing H/D. It is very uncertain to assume that this correlation is

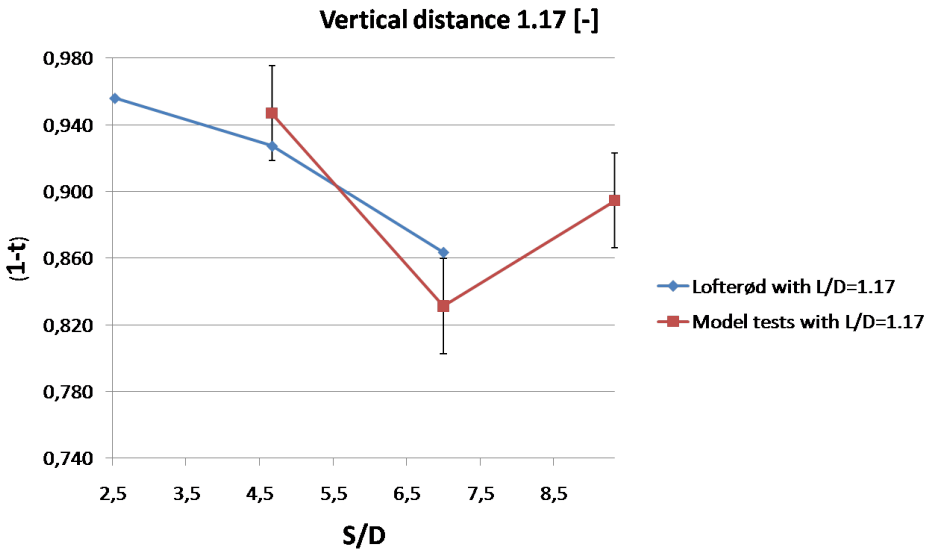

Figure 9.3: Comparison with Lofterød, fixed vertical position $L/D = 1.17$

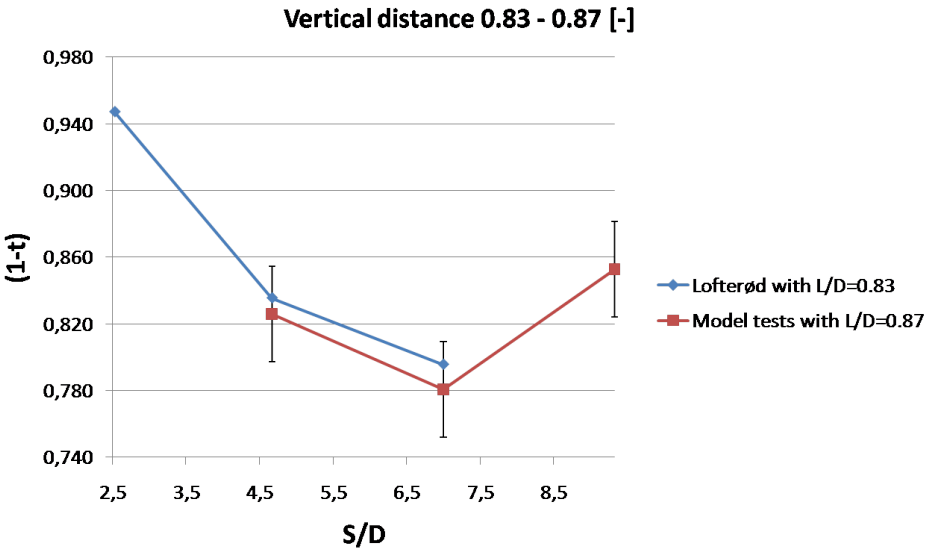

Figure 9.4: Comparison with Lofterød, fixed vertical position $L/D = 0.83 - 0.87$

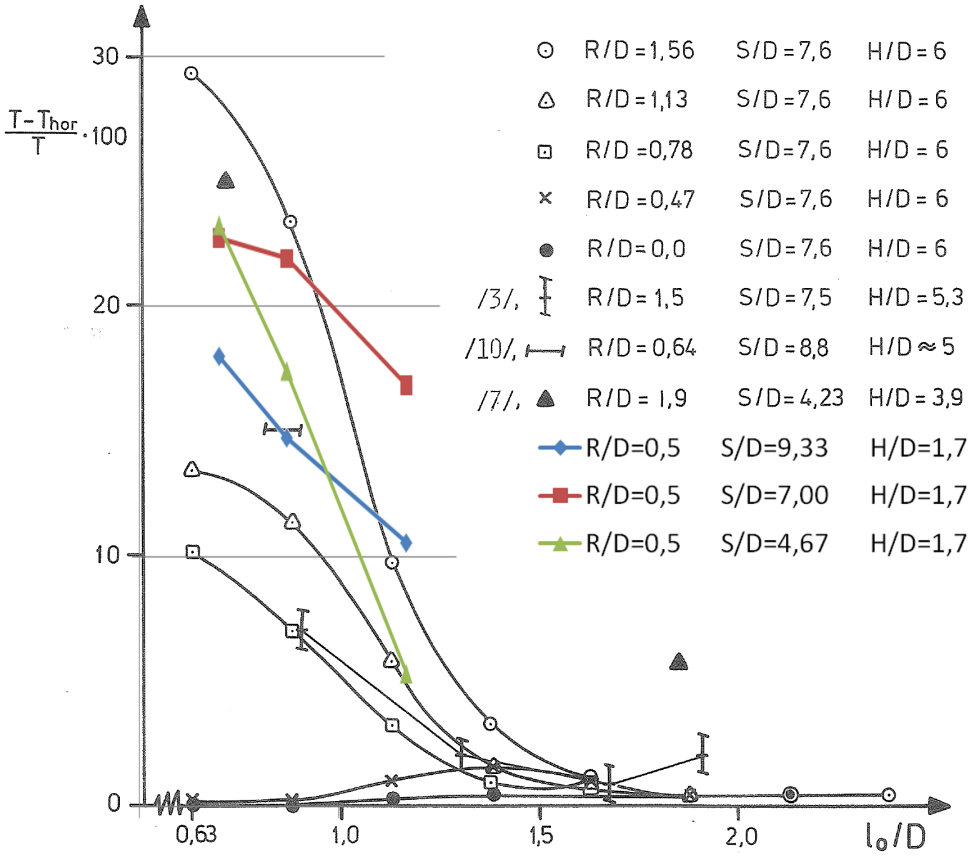

Figure 9.5: Comparison with Thon and Lehns experimental results

valid for significantly larger values of H/D, but due to increased friction with longer distance to the free surface the values of t will probably be higher in general for larger values of H/D.

It is interesting to notice the trend in 9.5 that the bilge radius, R, seems to be the most significant parameter for the results of Thon, with the largest values of t related to large values of R/D. The results of the model tests however, lies in the lowest part of the R/D selections yet having relatively large values of t. It is difficult to conclude with any specific pattern when comparing results, but 9.5 might suggest that the draught, H, has a significant influence on the thrust deduction t.

Another interesting phenomenon seen in 9.6 is that the deflection of slipstream centerline around bilge measured at the side of the pontoon, γ_m in Thon's results, seems to increase in the range $L/D = 0.63 - 1.5$ for a radius of $R/D = 0.47$. This radius is very close to the radius of the model tests in addition to the model tests' range $L/D = 0.7 - 1.17$ and $S/D = 7.6$ being within the measured values of the model tests. In theory, this increased deflection angle should result in a larger thrust loss, and consequently a lower $(1 - t)$, but this trend is not evident in the results of the model test in neither 6.4 or 6.3. As can be seen in 9.6 this phenomenon occurs only for the smallest values of R/D. Unfortunately the $R/D = 0.47$ is not included in Thon's results for other values of S/D, so it is difficult to conclude whether this should be expected in the this master's thesis' test results as well. However, Thon concludes that this particular effect is due to the distance $L/D \approx 1.4$ lets the slipstream be attracted towards the hull right before the bilge and thus having a very favorable incoming direction for large deflections over the bilge. Part two of Thon's experiment, the mathematical predictions, are described more thoroughly in

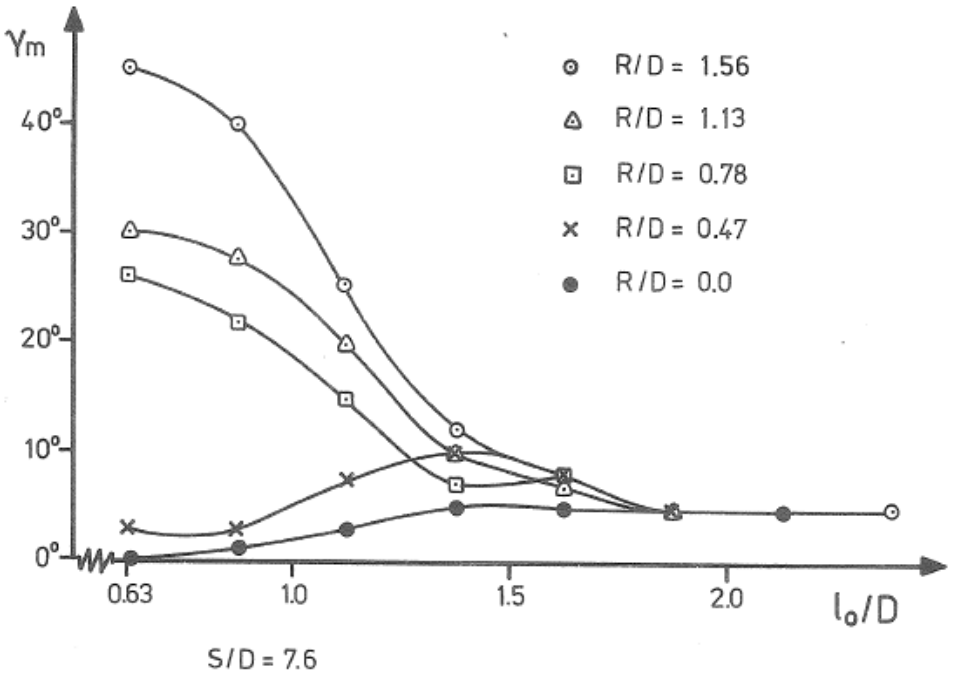

Figure 9.6: Deflection angles of Thon's results

9.3.3.

9.3 Comparison with Faltinsen's mathematical model

9.3.1 Author's and Faltinsen's numerical solutions

The deduction of the numerical solution to the force balance can be found in C.4 while the source code from Matlab is included in the attached DVD. In 9.7 the numerically predicted attachment lengths of the author are shown in addition to the attachment lengths presented from Faltinsen. Faltinsen's numerical results are digitalized from a figure originally plotted on a sheet of paper which is scanned and attached in D.2. The 7 shortest and slightly wobbly graphs in 9.7 are the numerical results from Faltinsen, while the 7 longer graphs are the numerical results of the author. The color codes for different angles α are the same for both Faltinsen's graphs and the author's. This comparison between the numerical solutions to Faltinsen's mathematical method by the author and by Faltinsen shows, as can easily be seen, little agreement in the results. In the numerical solutions in this subsection the parameter a is set to be equal to $a = L/D = 0.87$.

According to the author's numerical solution there will in practice be no Coanda effect on a normally sized model, and thus no thrust loss due to Coanda effect should therefore be present. As the experimental results shows the opposite and Faltinsen (1990) suggests otherwise as well, a thorough review of both the deducted theory and the numerical source code has been launched. It appears that Faltinsen's numerical solution is based on a slightly different deducted equation for the local radius of curvature, R. Recalling 3.28, there seems to be a difference factor of $\frac{1}{A}$ in the deducted expression for R used by Faltinsen. As a small test 3.28 is then altered by multiplying with the difference factor and the expression $R = \frac{4 \cdot A}{3} \cdot \frac{1}{\sqrt{h^2 - r_0^2}}$ in the numerical calculations yields the result presented in 9.8.

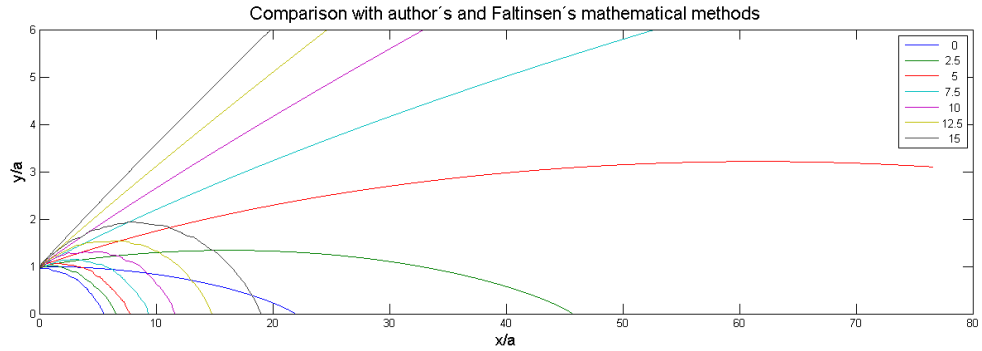

Figure 9.7: Comparison with authors and Faltinsen's numerical solutions

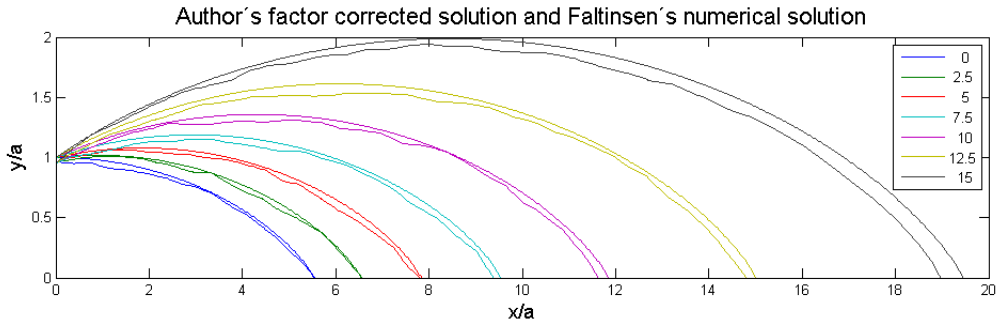

Figure 9.8: Comparison with factor corrected solution and Faltinsen's numerical solutions

As seen the resemblance with the slightly wobbly results of Faltinsen and the numerical factor corrected solution is striking. After a review of the deducted theory in 3.2 with NTNU personnel with a theoretical background on jet stream theory still no physical explanation for the difference factor has been obtained, and consequently the author's mathematical method stands but without consent with the experimental results.

9.3.2 Comparison with experimental results

A comparison between the calculated results with all three values of $a = L/D$ and show that there is practically no difference in predicted attachment lengths for any of the α.

Due to deviant results when solving the force balance numerically the experimental results will be compared with both predicted attachment lengths described in 9.3.1. When looking at the figures in 6.3 it seems quite clear that for nozzle angles $\alpha = 7.5°$ and $\alpha = 10°$ the thruster jet stream is not particularly in contact with the model bottom due to relatively high and constant values of $(1 - t)$. A small exception may be in 6.8, with $L/D = 1.17$, where the $(1 - t)$ for the $\alpha = 7.5°$ condition seems to drop when $S/D \rightarrow 9.33$, suggesting that the thruster jet stream could be close to an attachment of the jet centerline. A value $a = L/D = 1.17$ equals $a = 1.17 \cdot D = 0.176$ m and a value for $x = S/D = 9.33$ equals $x = 1.4$ m, which would suggest an attachment length a little above $x/a = 8$. Comparing this result with 9.8, which predicts a centerline attachment at $x/a \approx 9$, the numerical solution of Faltinsen seems to be quite accurate. Comparing the results with derived numerical model of the author in 9.7 show little consent in the predicted attachment length, as the predicted attachment length for $\alpha = 7.5°$ and $a = L/D = 1.17$ is $x/a = 580$.

The maximum size of the model bottom acting as a wall for the thruster jet is 1.4 m and the smallest value of $a = 0.105$ m. This means that when the predicted attachment length for a jet stream with an angle α is above $x/a \approx 13$ the jet stream should avoid the model hull and not leave a mark in the form of a sudden decrease in $(1 - t)$ in the experimental results. The derived numerical solution is therefore in practice predicting that this particular jet stream will not attach, which does not correspond well with the experimental results.

When observing the graphs for the condition $\alpha = 0°$, still in 6.3, it appears as though the jet stream has attached to the wall on all three horizontal conditions. The measurements for $S/D = 9.33$ is somewhat larger than expected and will not be used in any comparison. The two shorter values of S/D, however, show a constant and quite large thrust loss, and the assumption is that the situation for $S/D = 9.33$ is not different. Looking at 6.6 and 6.7 the experimental results show that the jet stream has attached to the model hull, based to the constant thrust loss measured for $S/D = 4.67$ and $S/D = 7.00$, already at $S/D = 4.67$, while in 6.8 with the largest vertical difference L/D the jet stream avoids the model hull for $S/D = 4.67$ but not $S/D = 7.00$. This may suggest that the attachment length for the jet stream of $\alpha = 0°$ is a little less than x/a with $x = 4.67 \cdot D$ for $a = 0.87 \cdot D$, meaning a little over $x/a \approx 5.4$. This corresponds very well with Faltinsen's numerical solution in 9.7, which predicts an attachment length of $x/a \approx 5.7$. The derived numerical solution, however, predicts an attachment length of $x/a \approx 22.5$ which in practice implies that no attachment will take place.

After two specific comparisons the mathematical method Faltinsen's numerical solution is a very good match with the experimental results. The derived numerical solution, however, does not seem to coincide with the measured thrust losses.

9.3.3 Comparison with Thon's mathematical model

The mathematical method derived from Faltinsen's private notes on the Coanda effect, Faltinsen, is the primary theoretical approximation in this master's thesis. However, a brief comparison with the mathematical method of Thon (1986) could provide further knowledge on the accuracy of the theoretical approaches on the Coanda effect. The setup and execution of Thon's experiment is described in 2.2, and the experimental results are described in 9.2. This mathematical method will not be derived or explained further, but can be found in Thon (1986), or originally in Teigen (1980).

The mathematical model predicts the path of the slipstream centerline and the distance from nozzle exit to attachment, and is given in 9.9, 9.10 and 9.11. The parameter l_0 of Thon equals the parameter L in this master's thesis, and with Thon's propeller diameter of $D_{Thon} = 0.08$ meter the values of l_0/D_{Thon} can be calculated. Thon has performed calculations for several l_0, but $l_0 = 0.05$, $l_0 = 0.07$ and $l_0 = 0.09$ will naturally be focused on due to the corresponding values of l_0/D_{Thon} are quite similar to the values of L/D in this master's thesis and should be valid for comparison with Faltinsen's mathematical method in 9.3. The three values of l_0 corresponds to $l_0/D_{Thon} = 0.625$, $l_0/D_{Thon} = 0.87$ and $l_0/D_{Thon} = 1.125$.

The predicted attachment lengths by Thon's mathematical model is calculated and given in 9.1. As seen the predicted attachment lengths of Thon is somewhat larger than the attachment lengths of Faltinsen's numerical solution, although not in the order of magnitude to be compared with the author's derived numerical solution. The behavior of Thon's mathematical model is quite different than of Faltinsen due to the attachment length increasing more rapidly with increasing angles α.

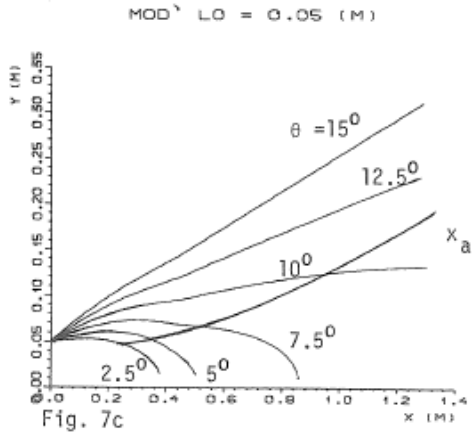

Figure 9.9: Thon's attachment results for $l_0/D_{Thon} = 0.625$

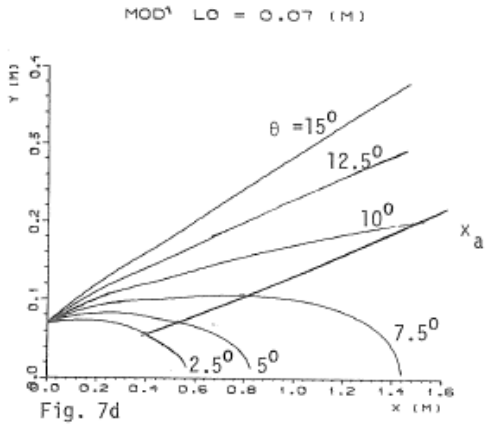

Figure 9.10: Thon's attachment results for $l_0/D_{Thon} = 0.87$

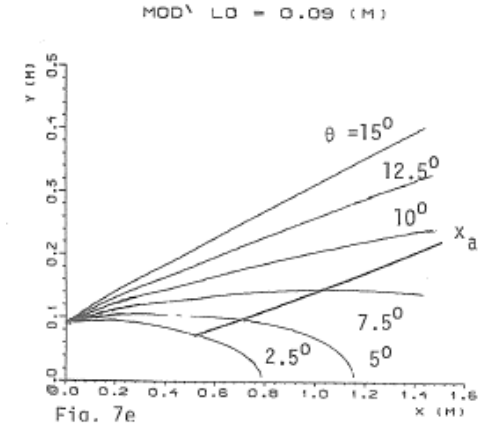

Figure 9.11: Thon's attachment results for $l_0/D_{Thon} = 1.125$

Table 9.1: Predicted attachment length by Thon's model

$D = 0.08$	Angles α		
Attachment	2.5	5	7.5
$l_0/D = 0.625$	8	12	17.4
$l_0/D = 0.875$	8.5	12.4	20.7
$l_0/D = 1.125$	8.9	12.8	-
Faltinsen	6.9	8.2	9.6

Chapter 10

Conclusions

10.1 Main conclusions

The overall objective in this master's thesis has been to investigate how certain parameters influence the thrust loss due to the Coanda effect. An experiment has been performed with this intention, and a mathematical model has been derived to compare results with. The model used in the experiment has a general form with flat bottom, straight side and a bilge connecting the shell together. In general the experimental results are plausible and to a large degree support theory. Some conclusions from the experimental and the mathematical results can be drawn:

1. Tilting the thruster nozzle angle 7.5° will effectively reduce the thrust loss with approximately 10 %. A further tilting of the nozzle shows little or no effect in reducing the thrust loss.
2. By increasing the vertical distance between thruster and hull the thrust loss is reduced. A minor change in vertical distance can significantly improve the $(1-t)$, depending on other parameters.
3. Tilting the thruster nozzle angle does not cause more than $1-3$ % thrust loss for the least exposed conditions of Coanda effect losses.
4. Decreasing the horizontal distance between thruster and model side will in general reduce the thrust loss with approximately 5 % for a tilted thruster nozzle. Without tilting the thruster changing the horizontal distance between thruster and side has little effect for the horizontal range in this experiment.
5. Comparisons with similar experiments do show that it is difficult to replicate the results, even with initially equal parameters.
6. The mathematical model with Faltinsen's numerical solution shows a very good accuracy with predictions of the attachment length compared with the experimental results.
7. The maximum measured thrust loss during the experiment is 24 %.
8. The thrust loss neither increases nor decreases with varying the thrust force on the propeller within the range $10-17.5$ rps.
9. The position of the thruster plays a decisive role for the influence the Coanda effect has on a jet stream.

10.2 Recommendations for further work

After this investigation of parameters influencing the thrust loss due to Coanda effect, some questions have been answered while new questions have arisen. The list of recommendations for further work is as follows:

1. First of all, more experiments with similar parameters and setup is needed to investigate the validity of the model tests' results. This will help remove scatter results and improve the accuracy of the conclusions drawn.

2. As previously mentioned the downwards tilting of the thruster nozzle has proven effective in reducing the thrust loss. Tilting the thruster nozzle more than 7.5°, however, does not provide an additional decrease in the thrust loss. It is recommended that the range in nozzle angles, $\alpha = 0 - 7.5°$, is investigated further to see if $\alpha = 7.5°$ can be reduced without increasing the thrust loss. Recalling the discussion in 7.3 on whether the optimal results in this setup is in sum optimal for a vessel's life cycle the choice of thruster tilting angle will always be a trade off. If the thrust loss can be shown to not decrease with a minor decrease in α this would be of great value in the further investigation of the Coanda effect.

3. Again recalling the discussion in 7.3 a further experimental study of the Coanda effect under a more realistic environment regarding waves and current is recommended. When knowing the thrust loss for a certain condition it would be interesting to see how thrust loss develops when introducing waves in the test basin.

4. Replacing the model used in this experiment with a complete submerged hull of for instance a semi submersible platform and perform studies of an initially known condition, only with rotating the thruster 360°, would be a significant continuation of this experiment as well. This would provide further information to which parameters that can reduce the thrust loss.

5. In this experiment the bilge radius has been fixed to $R/D = 0.5$, as opposed to both Lofterød (2007) and Lehn (1985). A further investigation with several bilge radii included in combination with the investigated parameters would provide additional information regarding which geometric conditions where an additional awareness of the Coanda effect is needed.

6. As seen in 9.1 the results of Lofterød (2007) vary compared to the results from the model tests. A known geometric difference between the two experiments is the pitch ratio of the propeller used. An experiment on the Coanda effect where the pitch ratio is included as a parameter would be interesting to investigate whether this influences the thrust loss due to Coanda effect.

7. The threads glued on the model bottom centerline did not provide information regarding the attachment of the thruster jet to the hull, as the threads were hard to spot in the video footage afterwards. Performing a similar experiment with a better solution for this, for instance placing larger threads with more contrast color and placing a camera directly underneath the model, would be beneficial for gaining knowledge on the attachment length and for verifying mathematical models.

Nomenclature

$(1-t)$	Non dimensional measurement of remaining thrust, see also t
α	Tilting angle of thruster
ϵ_0	Virtual kinematic viscosity
η	Radius ratio
$\mathbb{F}$	Force acting on a cross section of the jet
$\mathbb{X}$	Real part of force on jet in axial direction
$\mathbb{Y}$	Real part of force on jet in y-direction
ν	Kinematic viscosity
π	Pi
ρK	Constant kinematic momentum
ρ	Fluid density
τ	Reynolds stress
A	Constant in relation to radius ratio
a	Distance to sink from wall
B	Limit for outer axial velocity of jet
b	Radial distance to $u = \frac{1}{2} \cdot u_m$
C	Strength of sink
c	Cross section body contour
D	Thruster diameter
e_B	Bias elemental error
e_P	Precision elemental error
e_T	Total elemental error
$F_{attraction}$	Attraction force on the jet
$F_{centrifugal}$	Centrifugal force of the jet
F_{prop}	Force applied on the propeller
F_{tot}	Total force on the model

h	Distance to center of jet
i	Standard imaginary unit
p	Pressure
$P_{\overline{x}}$	Precision limit for the mean of a number of repetitions
Q	Volume flow
R	Local radius of curvature
r	Radial distance to center of jet
r_0	Radius of nozzle exit
Re	Reynolds number
s	Axial distance from outlet
s_0	Distance to the virtual origin of jet
S_x	Standard deviation of a sample population
t	Thrust deduction
t	Weight in student's t-distribution
U	Velocity in a flow
u	Mean velocity in axial direction
u'	Velocity fluctuations in axial direction
u_m	Maximum velocity located at jet centerline
u_{ent}	Axial entrainment velocity
v	Mean velocity in radial direction
v'	Velocity fluctuations in radial direction
v_r	Radial velocity
w	Complex velocity of the sink
x	Axial distance
z	Position of sink

Bibliography

Report of the Panel on Validation Procedures, 1990. International Towing Tank Conference.

J. V. Aarsnes and S. Steen. Experimental methods in marine hydrodynamics. Marine Technology Centre Trondheim, Norway, 2008.

G. N. Abramovich. The theory of Turbulent jets. M.I.T. Press, Massachusetts, 1963.

C. Allery, S. Guerin, A. Hamdouni, and A. Sakout. Experimental and numerical POD study of the Coanda effect used to reduce self-sustained tones. LEPTAB, Université de La Rochelle, 2002.
`http://www.sciencedirect.com`.

J. Brix. Maneuvering technical manual. Kessler Verlagsdruckerei, Bobingen, 1993.

Discovery Channel. Pioneers of flight
`http://www.discoverychannel.co.uk/flight/pioneers_of_flight/henri_coanda/index.shtml`. Accessed December 9, 2009.

O. M. Faltinsen. Coanda effect. Unpublished notes acquired from Faltinsen 02.12.09.

O. M. Faltinsen. Sea loads on ships and offshore structures. Cambridge University Press, 1990.

H. H. Fernholz. The deflection of free jets at convexly curved walls (Coanda effect). Technical report, National Research Council of Canada, 1971.

H. H. Fernholz and R. Willie. Report on the first European Mechanics Colloquium, on the Coanda effect. Technical report, Hermann Föttinger Institut, Technische Universität Berlin, 1965.

H. Fjørtoft. Thrust loss on azimuthing thrusters due to coanda effect. Project thesis prior to this master's thesis, delivered 22.12.09.

ITTC. ITTC Recommended Procedures)
`http://ittc.sname.org/2002_recomm_proc/7.5-02-01-03.pdf`. Accessed May 11, 2010.

N. E. Kotsovinos. A note on the spreading rate and virtual origin of a plane turbulent jet. Journal of Fluid Mechanics, 77(2):305 – 311, 1976.
`http://journals.cambridge.org`.

H. Köster and R. Löhr. Untersuchung der Umlenkung eines ebenen Strahles durch einen Kreiszylinder (Coanda-Effekt). Institut für Aerodynamik der DFL Braunschweig, 1964.

P. K. Kundu and I. M. Cohen. Fluid mechanics. Academic press, 2nd edition edition, 2002.

H. Lamb. Hydrodynamics. Cambridge University Press, 6th edition edition, 1932.

E. Lehn. On the propeller race interaction effects. Technical report, MARINTEK, 1985.

A. Lofterød. Coanda-Effect of Azimuthing Thrusters beneath a Hull. Master's thesis, 2007.

K. Minsaas and S. Steen. Propell og foilteori. Marine Technology Centre Trondheim, Norway, 2005.

NTNU. Marine Cybernetics Laboratory (MCLab) `http://www.ntnu.no/imt/lab/kybernetikk`. Accessed April 29, 2010.

R. Rajaratnam. Turbulent jets. Elsevier Scientific Publishing Company, 1976.

A. Revuelta, A. Sánchez, and A. Liñán. The virtual origin as a first-order correction for the far-field description of laminar jets. Physics of fluids.

H. Schlichting. Boundary layer theory. Mc. Graw - Hill Book company, 1968.

J. Slomski and T. Marino. Journal Article 153 `http://www.fluent.com/solutions/articles/ja153.pdf`. Accessed December 9, 2009.

I. J. Sobey. Introduction to interactive boundary layer theory. Oxford University Press Inc., 2000.

P. S. Teigen. Propeller induced forces on towed structures. Technical Report R.107.80, NFSI, 1980.

H. J. Thon. Deflection of the propeller slipstream. Technical report, MARINTEK, 1986.

M. Uddin and A. Pollard. Self-similarity of coflowing jets: The virtual origin. Physics of fluids.

R. H. Walpole, R. H. Myers, S. L. Myers, and K. Ye. Probability & Statistics for Engineers & Scientists. Pearson Prentice Hall, 8th edition edition, 2007.

F. M. White. Fluid mechanics, fifth edition. The McGraw-Hills Companies, Inc., 2003.

Appendix A

Experimental results

A.1 Dependency on rps for different horizontal conditions and nozzle angles

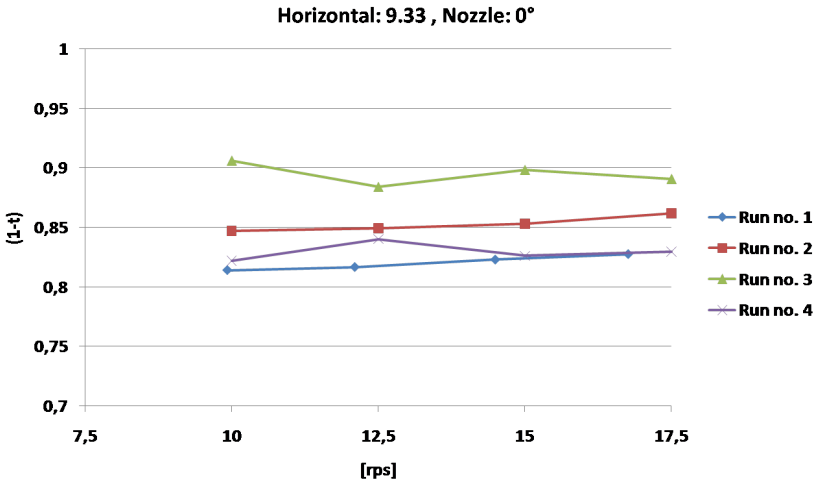

Figure A.1: Dependency on rps for $L = 9.33[-]$ and $\alpha = 0°$

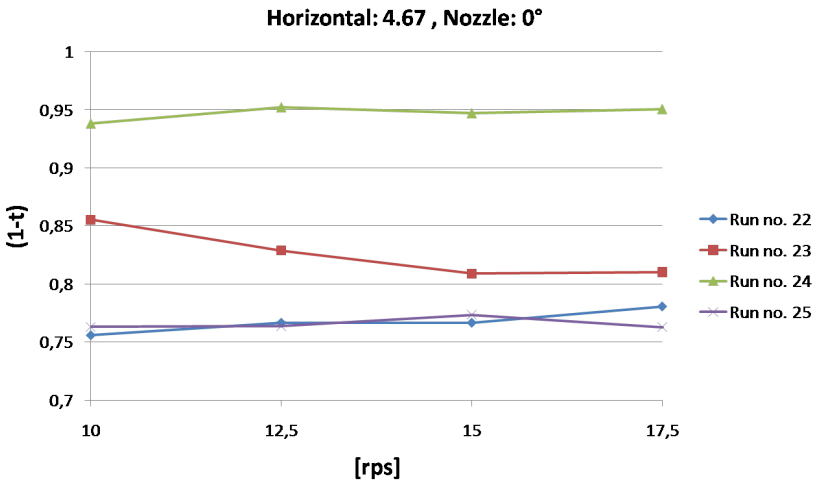

Figure A.2: Dependency on rps for $L = 4.67[-]$ and $\alpha = 0°$

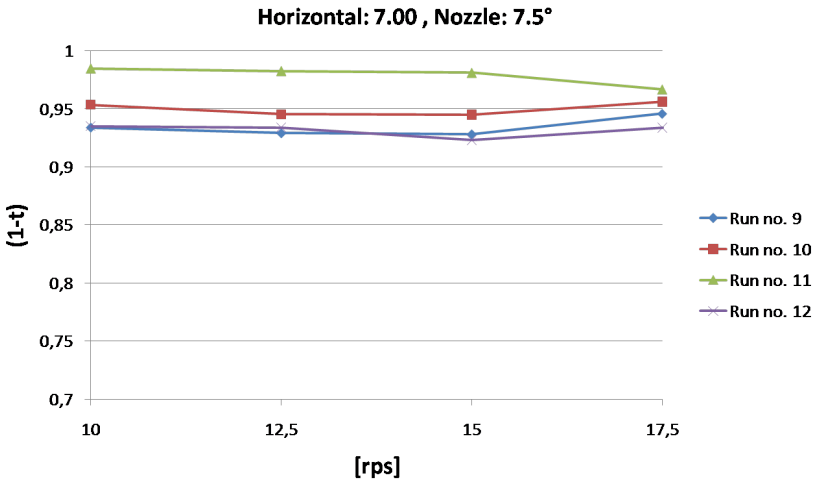

Figure A.3: Dependency on rps for $L = 7.00[-]$ and $\alpha = 7.5°$

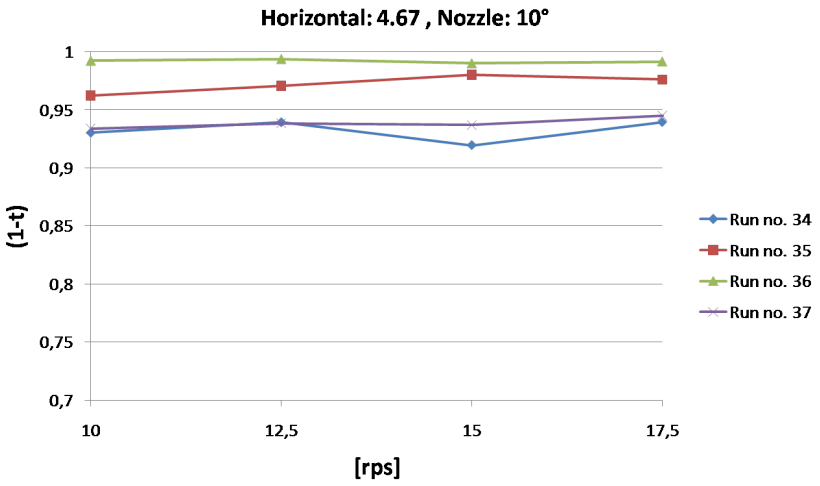

Figure A.4: Dependency on rps for $L = 4.67[-]$ and $\alpha = 10°$

A.2 Measurements of current in the tank

Table A.1: Measured current before each run

Run no.	Initial $F_{tot,curr}$	Ending $F_{tot,curr}$	Initial $F_{prop,curr}$	Ending $F_{prop,curr}$
1	0.005723	0.324876	0.006553	-0.00748
2	-0.09037	1.81344	0.01448	-0.07868
3	-0.03394	0.412052	0.044163	0.165164
4	0.024203	-0.63102	0.0174	-0.16306
5	-0.00677	-0.00701	-0.00437	-0.05951
6	0.008673	1.820088	0.00095	-0.13563
7	-0.0932	3.064952	-0.00068	-0.09166
8	-0.03222	-1.08014	-0.00382	-0.12299
9	-0.01537	0.111708	0.001657	-0.07591
10	0.02531	-0.19278	0.001733	-0.10634
11	0.385153	1.042972	-0.001	-0.17524
12	0.015953	-0.74373	0.00277	-0.1153
13	-0.03044	-0.18118	0.016547	-0.12352
14	0.272183	-0.65128	-0.23069	-0.26097
15	-0.08323	1.619608	-0.01547	-0.07293
16	0.029717	-0.17948	0.022897	-0.06027
17	0.001083	-0.15307	0.022533	-0.0656
18	-0.26963	0.261528	-0.04878	-0.06469
19	-0.01643	-0.28235	-0.00686	-0.11859
20	0.996233	0.179852	0.76595	-0.07819
21	0.00946	-0.35461	0.003787	0.121428
22	-0.03391	-0.46699	0.336157	0.351368
23	-3.6068	-3.99336	0.496683	0.477208
24	-0.57703	-0.48925	-1.03571	-0.91734
25	0.017077	0.379736	0.001123	0.155164
26	0.010303	-0.27035	0.009337	-0.10992
27	-0.05273	-0.78024	0.017647	-0.12573
28	-0.01052	-1.18064	-0.00179	-0.11895
29	-0.00407	-0.51973	0.027243	-0.09874
30	0.008203	-0.75264	0.004647	-0.07445
31	0.021323	-0.44721	0.002877	-0.11325
32	0.018643	-0.10896	-0.00151	-0.10824
33	-0.00738	-0.48657	0.026167	-0.21774
34	0.051213	-0.16711	0.01269	0.163664
35	-0.02084	-0.3456	0.00288	0.010128
36	-0.03414	-0.362	0.012617	-0.00131
37	0.132397	-0.40532	0.15804	0.041504

A.3 Decay test in air

A decay test in air has been performed to find the resonance frequency of the model. In A.5 the measured responses are shown. The resonance frequency has been calculated to be 4.9 Hz. Plots and calculations have been done in Matlab, and the source code is found in the attached DVD.

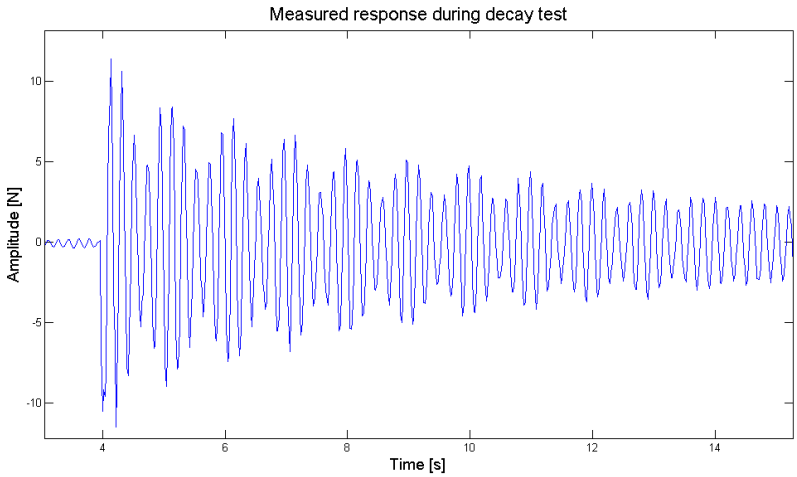

Figure A.5: Measured response during decay test in air

A.4 Open water diagrams

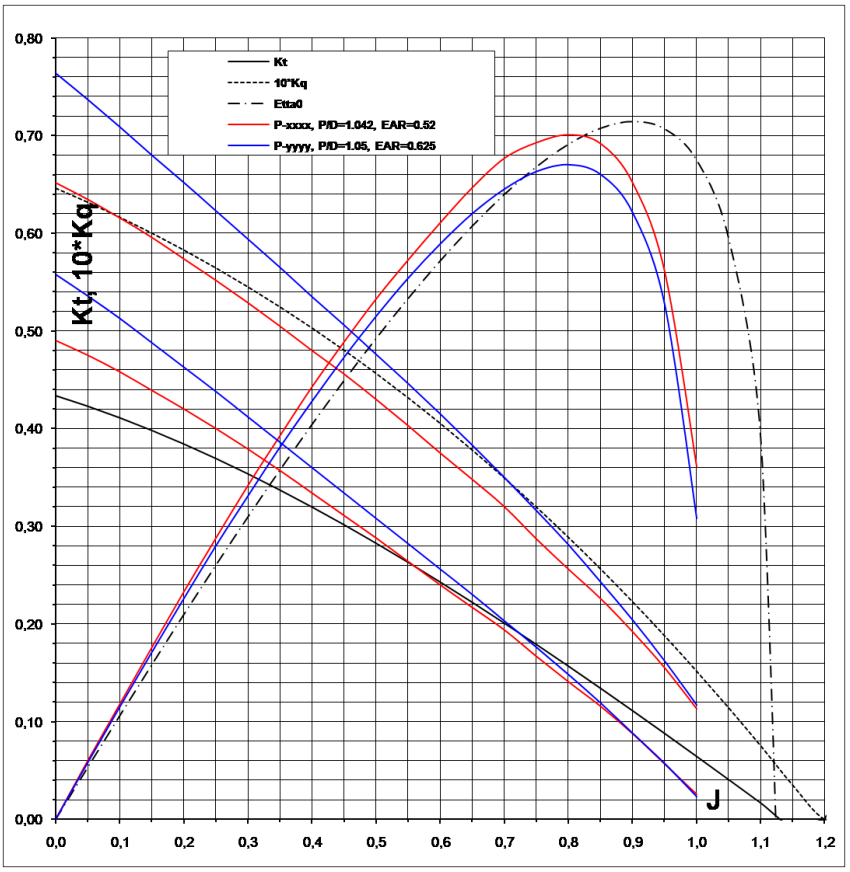

Figure A.6: Open water diagram for the Wageninger B series

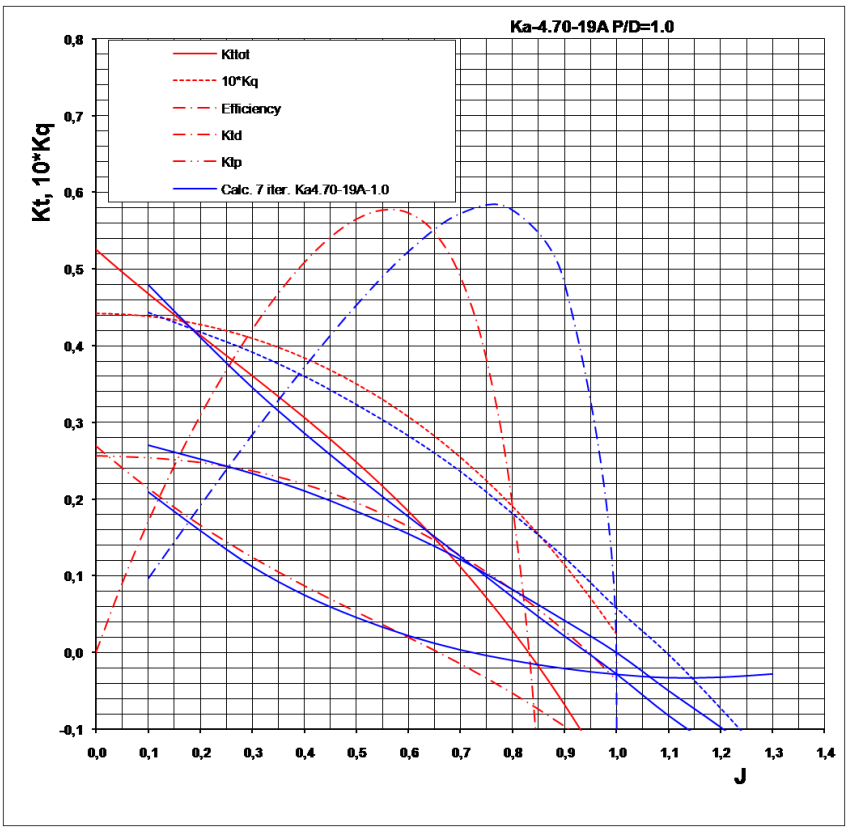

Figure A.7: Open water diagram for the Ka4-70 series

Appendix B

Previous experiments

B.1 Lehns experiment

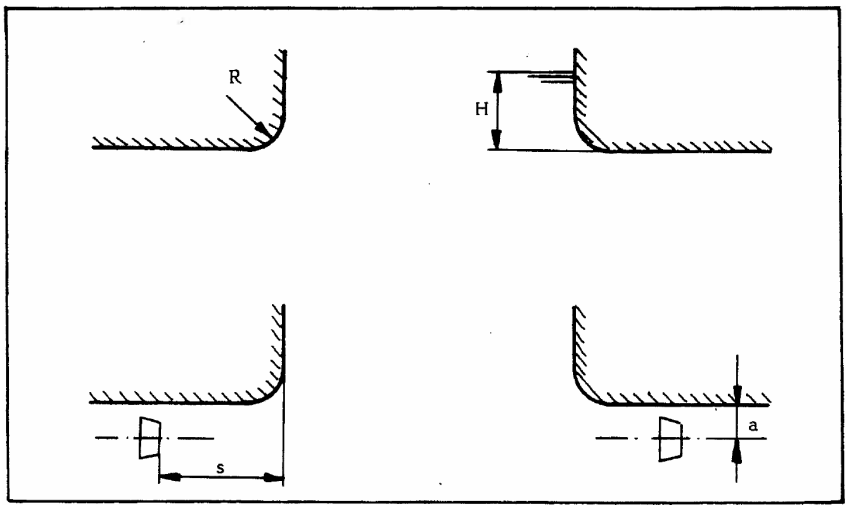

Figure B.1: Explanatory sketch of Lehns parameters

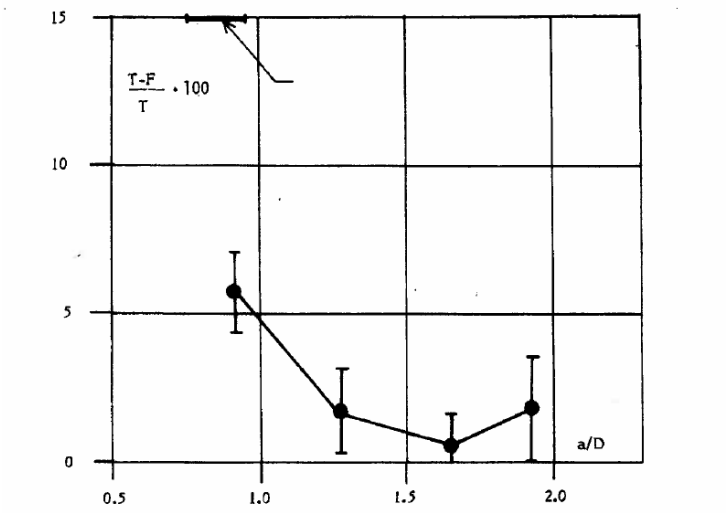

Figure B.2: Lehn's Coanda losses versus distance between thruster and model bottom

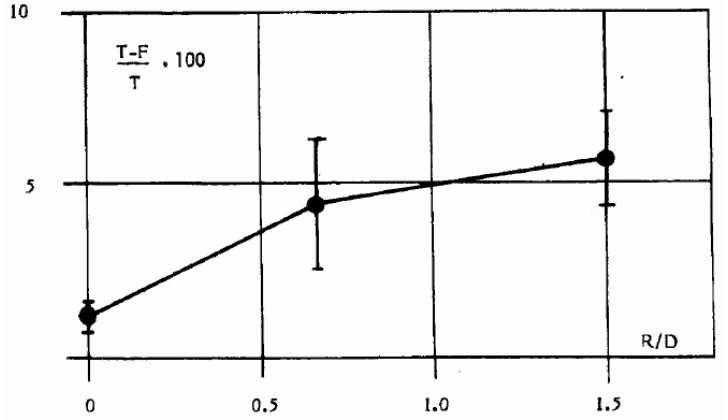

Figure B.3: Lehn's Coanda losses versus bilge radius

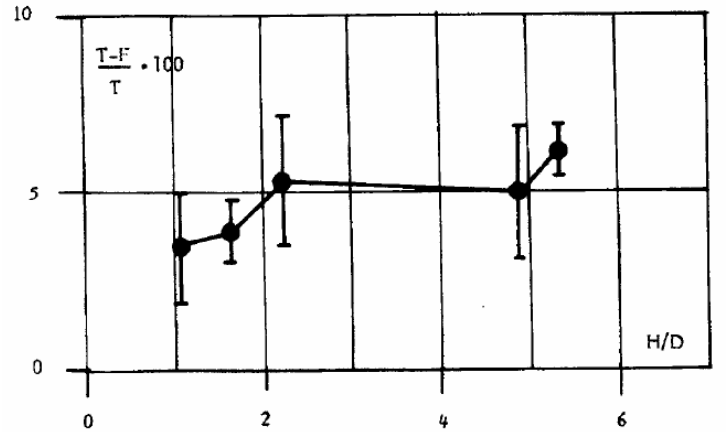

Figure B.4: Lehn's Coanda losses versus draught

B.2 Figures related to Thon's experiment

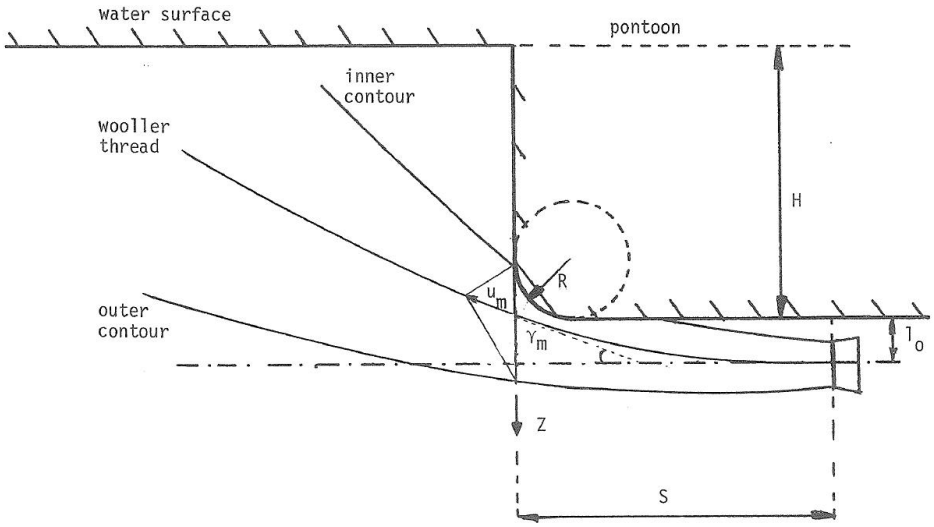

Figure B.5: Explanatory sketch of part one if Thon's experiment

$l_{o/D}$ = 0.625 - 2.875, increment 0.25

$\theta = 0^o$-15^o, increment 2.5^o, for $l_{o/D} \leq 1.375$

$\theta = 0^o$ for $l_{o/D} > 1.375$

Figure B.6: Test conditions for part one in Thon's experiment

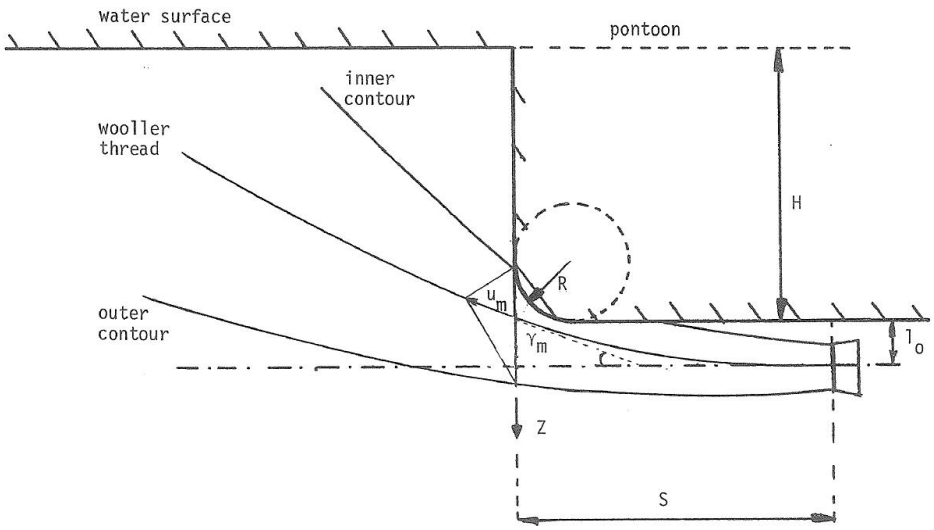

Figure B.7: Explanatory sketch of part two if Thon's experiment

Appendix C

General deductions

C.1 Deduction of velocities for turbulent circular jet

Schlichting Schlichting (1968) proposes a solution for a laminar circular jet. For most practical cases the circular jet is turbulent, but the laminar case can be developed to be valid for turbulent cases as well. The jet spreads outwards in the downwards direction along the x-direction from 3.4 owing to the influence of friction. The velocity in the center of the jet decreases in the same direction. The pressure gradient, $\frac{\partial p}{\partial x}$, is neglected the constant pressure in the surrounding fluid impresses itself on the jet. This leads to the conclusion that the total momentum, J, in the x-direction remains constant and thus, is independent of the distance to the orifice, x. 3.6 shows the axisymmetric jet with directions and variables.

Having assumed a constant pressure the flux of momentum then becomes constant in the direction of x:

$$J = 2\pi\rho \int_0^\infty u^2 \cdot y \, \mathrm{d}y = constant \tag{C.1}$$

Under the usual boundary-layer simplifications the equation of motion in the direction of x can be written as:

$$u\frac{\partial u}{\partial x} + v\frac{\partial u}{\partial y} = \nu \frac{1}{y}\frac{\partial}{\partial y}\left(y\frac{\partial u}{\partial y}\right) \tag{C.2}$$

$$\frac{\partial u}{\partial x} + \frac{\partial v}{\partial y} + \frac{v}{y} = 0 \tag{C.3}$$

The boundary conditions are:

$$y = 0 \qquad : v = 0; \frac{\partial u}{\partial y} = 0; \tag{C.4}$$

$$y = \infty \qquad : u = 0 \tag{C.5}$$

The assumptions that the velocity profiles $u(x, y)$ are similar and the width of the jet is proportional to x^n are made. Further, $\psi \sim x^p F(\eta)$ with $\eta = \frac{y}{x^n}$.

The two exponents, p and n, can be found by looking back on C.1 and C.2. The momentum in C.1 must be independent of x, as previously stated, and the inertia and frictional terms in C.2 must be of the same order of magnitude. This leads to the following relations:

$$u \sim x^{p-2n} \tag{C.6}$$

$$\frac{\partial u}{\partial x} \sim x^{p-2n-1} \tag{C.7}$$

$$\frac{\partial u}{\partial y} \sim x^{p-3n} \tag{C.8}$$

$$\frac{1}{y}\frac{\partial}{\partial y}\left(y\frac{\partial u}{\partial y}\right) \sim x^{p-4n} \tag{C.9}$$

The following equations for p and n reads:

$$2p - 4n + 2n = 0 \tag{C.10}$$

$$2p - 4n - 1 = p - 4n \tag{C.11}$$

$$\Downarrow \tag{C.12}$$

$$p = n = 1 \tag{C.13}$$

The value of p and n can now be put into: $\psi = \nu x F(\eta)$ and $\eta = \frac{y}{x}$. From this follows the velocity components:

$$u = \frac{\nu}{x}\frac{F'}{\eta}; v = \frac{\nu}{x}\left(F' - \frac{F}{\eta}\right) \tag{C.14}$$

Having obtained expressions for u and v these can now be inserted into C.2 to find the following expression for the stream function:

$$\frac{FF'}{\eta^2} - \frac{F'^2}{\eta} - \frac{FF''}{\eta} = \frac{d}{d\eta}\left(F'' - \frac{F'}{\eta}\right) \tag{C.15}$$

This equation can be integrated once, and the result is:

$$FF = F' - \eta F'' \tag{C.16}$$

Now, to find a particular solution to C.16 boundary conditions have to be introduced. First, at the slot, when $y = 0$ then u will be at its maximum, $u = u_m$, and the jet has not yet started to fan out, meaning $v = 0$. From this follows that $\eta = 0$ and that $F' = F = 0$ consequently. Going back to C.14, it is clear that since u is an even function $\frac{F'}{\eta}$ must be even, F' must be odd and F even.

When it comes to the expansion of F in power of η, the constant term disappears due to the fact that $F(0) = 0$. This determines one constant of integration. The second constant of integration is denoted γ. If $F(\eta)$ is a solution of C.16 then $F(\gamma\eta) = F(\xi)$ is a solution as well. C.16 can now be rewritten into:

$$F\frac{\mathrm{d}F}{\mathrm{d}\xi} = \frac{\mathrm{d}F}{\mathrm{d}\xi} - \xi\frac{\mathrm{d}^2F}{\mathrm{d}\xi^2} \tag{C.17}$$

A particular solution which satisfies this equation along with the previously stated boundary condition that $F = F' = 0$ for $\eta = 0$ is presented below in C.18:

$$F = \frac{\xi^2}{1 + \frac{1}{4}\xi^2} \tag{C.18}$$

This result can be inserted into C.14 for u and v. Here $\xi = \gamma\frac{y}{x}$.

$$u = \frac{\nu}{x}\gamma^2\frac{1}{\xi}\frac{\mathrm{d}F}{\xi} = \frac{\nu}{x}\frac{2\gamma^2}{\left(1 + \frac{1}{4}\xi^2\right)^2} \tag{C.19}$$

$$v = \frac{\nu}{x}\gamma\left(\frac{\mathrm{d}F}{\mathrm{d}\xi} - \frac{F}{\xi}\right) = \frac{\nu}{x}\gamma\frac{\xi - \frac{1}{4}\xi^3}{\left(1 + \frac{1}{4}\xi^2\right)^2} \tag{C.20}$$

Recalling C.1 and C.20, it is possible to calculate the constant J expressed with γ:

$$J = 2\pi\rho\int_0^\infty \frac{\nu}{x}\frac{2\gamma^2}{\left(1 + \frac{1}{4}\gamma\frac{y}{x}^2\right)^2}^2 \cdot y\,\mathrm{d}y \tag{C.21}$$

$$= (2\pi\rho\frac{2\nu}{x}^2\gamma^4)\int_0^\infty \frac{1}{\left(1 + (\frac{\gamma}{2x})^2y^2\right)} \cdot y\,\mathrm{d}y \tag{C.22}$$

$$= (2\pi\rho\frac{2\nu}{x}^2\gamma^4)\left[\frac{y}{\left(1 + (\frac{\gamma}{2x})^2y^2\right)^{-3}} \cdot \frac{-1}{6(\frac{\gamma}{2x})^2}\right]_0^\infty \tag{C.23}$$

$$= \frac{-16\pi}{3}\rho\nu^2\gamma^2\left[0 - 1\right] \tag{C.24}$$

$$J = \frac{16}{3\pi}\rho\gamma^2\nu^2 \tag{C.25}$$

The jet momentum, J, can also be expressed with the kinematic momentum, $K' = \frac{J}{\nu}$. γ can be determined by solving $J = K'\rho = \frac{16}{3\pi}\rho\gamma^2\nu^2$. The value of $\gamma = \sqrt{\frac{3}{16\pi}}\sqrt{\frac{K'}{\nu}}$. Inserted into C.20 u and v can be expressed on a form only containing kinematic viscosity, ν, and kinematic momentum, K':

$$u = \frac{3}{8\pi}\frac{K'}{\nu x}\frac{1}{\left(1 + \frac{1}{4}\xi^2\right)^2} \tag{C.26}$$

$$v = \frac{1}{4}\frac{3}{\pi}\frac{K'}{x}\frac{\xi - \frac{1}{4}\xi^3}{\left(1 + \frac{1}{4}\xi^2\right)^2} \tag{C.27}$$

Inserting γ into $\xi = \gamma\frac{y}{x}$ gives:

$$\xi = \gamma\frac{y}{x} = \sqrt{\frac{3}{16\pi}}\sqrt{\frac{K'}{\nu}}\frac{y}{x} \tag{C.28}$$

In Schlichting (1968) Schlichting states the power laws regarding for the increase in width and

the decrease in center-line velocity in terms of distance x for problems of free turbulent flow. These power laws are given in C.1.

	laminar		turbulent	
	width b	centre-line velocity u_{max} or u_1	width b	centre-line velocity u_{max} or u_1
Free jet boundary	$x^{1/2}$	x^0	x	x^0
Two-dimensional jet	$x^{2/3}$	$x^{-1/3}$	x	$x^{-1/2}$
Circular jet	x	x^{-1}	x	x^{-1}
Two-dimensional wake	$x^{1/2}$	$x^{-1/2}$	$x^{+1/2}$	$x^{-1/2}$
Circular wake	$x^{1/2}$	x^{-1}	$x^{+1/3}$	$x^{-2/3}$

Figure C.1: Power laws for the increase in width and for the decrease in center-line velocity in terms of distance x.

As seen in C.1 the width of the jet, b, is proportional to x for both a two-dimensional and a circular jet. The center-line velocity, however, is proportional to x^{-1} for a circular jet, as opposed to $x^{-1/2}$ for a two-dimensional jet. The virtual kinematic viscosity for the circular jet thus becomes:

$$\epsilon_\tau = \kappa_1 \cdot b \cdot U \sim x^0 = constant = \epsilon_0 \tag{C.29}$$

The fact that ϵ_0 stays constant over the whole of the jet leads to the conclusion that the velocity distribution becomes formally the same as for the situation with the laminar jet described earlier in this chapter. The only alteration needed is to replace the kinematic viscosity for the laminar jet, ν with the virtual kinematic viscosity for the turbulent flow, ϵ_0. The constant kinematic momentum is denoted K and is defined in general in C.30. Recalling C.26, C.27 and C.28, u, v and η can now be obtained for the circular jet:

$$K = 2\pi \int_0^\infty u^2 y \, \mathrm{d}y \tag{C.30}$$

$$u = \frac{3}{8\pi} \frac{K}{\epsilon_0 x} \frac{1}{\left(1 + \frac{1}{4}\eta^2\right)^2} \tag{C.31}$$

$$v = \frac{1}{4} \frac{3}{\pi} \frac{K}{x} \frac{\eta - \frac{1}{4}\eta^3}{\left(1 + \frac{1}{4}\eta^2\right)^2} \tag{C.32}$$

$$\eta = \sqrt{\frac{3}{16\pi}} \sqrt{\frac{K}{\epsilon_0}} \frac{y}{x} \tag{C.33}$$

C.2 The virtual origin

The jet flow far downstream of the transient region of the jet resembles remarkably a model of a flow induced by a point source. The asymptotic solution seems to improve when this point source is moved upstream of the jet outlet, according to Uddin et. al. (2007) Uddin and Pollard, and this is what is called the virtual origin of the jet. According to Revuelta et. al. (2002) Revuelta et al. the virtual origin is dependent on the shape of the initial jet velocity profile for a laminar jet, but concludes that there also are similarities for the case of a turbulent jet.

C.2.1 Previous experimental results of virtual origin

In general there is a broad agreement of the existence of a virtual origin, although the location of it is a matter of discussion. Kotsovinos Kotsovinos (1976) has performed a literature review regarding the location of the virtual origin. A central equation in determining the virtual origin is C.34, collected from Kotsovinos Kotsovinos (1976):

$$\frac{b(x)}{D} = K_1 \cdot \left(\frac{x}{D} + K_2\right) \tag{C.34}$$

Here $b(x)$ represent the half widths, i.e. where $u = \frac{1}{2} \cdot u_m$, K_1 is a measure of the spreading rate of the jet and K_2 determines the location of the virtual origin, x_0, as shown in C.35. D is the diameter of the jet outlet.

$$x_0 = -K_2 \cdot D \tag{C.35}$$

Kotsovinos has collected values of K_1 and K_2 in the literature, and is presented in C.2 taken from Kotsovinos Kotsovinos (1976).

Experimenter(s)	Slot aspect ratio	l_{min}/D	l_{max}/D	l_{max}/W	$Re \times 10^{-3}$	K_1	K_2
Albertson *et al.* (1950)	720–5760	24	2300	1·20	10	0·128	—
Flora & Goldschmidt (1969)	50	—	90	1·80	20	0·11	0·0
Förthmann (1934)	21	0	25	1·19	70	0·096	0·60
Goldschmidt & Eskinazi (1966)	16	15	67	4·20	16	0·099	−0·66
Heskestad (1965)	120	47	155	1·30	35	0·11	−4·2
Jenkins & Goldschmidt (1973)	24	30	60	2·5	14	0·088	4·5
Kotsovinos (1975)	54	20	94	1·45	2	0·109	−2·5
	13	14	37	2·85	2	0·087	6·5
Mih & Hoopes (1972)	59	—	300	5·08	20	0·117	—
Miller & Comings (1957)	40	0	40	1·0	20	0·096	1·6
Nakaguchi (1961)	133	—	100	0·75	10	0·106	0·3

Figure C.2: Review of experimental values related to the virtual origin

As seen in C.2 there are large variations in K_2, and the conclusions ranges from both $6.5 \cdot D$ upstream to $2.5 \cdot D$ downstream of the jet outlet. According to Uddin et. al. Uddin and Pollard a location of the virtual origin downstream of the jet outlet can be explained through a back flow at the origin. Abramovich Abramovich (1963) have gathered earlier German and Russian results and obtained a value $K_2 = 2.2$ meaning that the virtual origin is located $2.2 \cdot D$ upstream of the jet outlet. Due to large uncertainties the virtual origin is by some suggested to be located at the jet outlet, as for Albertson et. al. seen in C.2, also described in Rajaratnam Rajaratnam

(1976). Kotsovinos himself concludes with a value $K_2 \approx 2.5$, meaning that the virtual origin is located approximately $2.5 \cdot D$ upstream of the jet outlet. Kotsovinos also claims to have found a non-linear relation between K_1 and K_2 explaining the large variations of different experimenters. This conclusion is questioned in the more recent Uddin et. al. Uddin and Pollard, who have performed Large Eddy Simulations on the subject, and this topic will be left undiscussed in this master's thesis.

Lehn Lehn (1985) has, through curve fitting of collected results, obtained an empirical formula for $\frac{b}{D}$ given in C.36. Here b stands for the half-widths, as for all referenced results in this section. By setting the value of $b = 0$ one would obtain the x-value at the origin. Doing so, Lehn obtains the location of the virtual origin to be approximately $x_0 \approx 4.5 \cdot D$ upstream of the jet outlet.

$$\frac{b}{D} = 0.39 + 0.0875 \cdot \frac{x}{D} \tag{C.36}$$

C.2.2 Calculated location of virtual origin

Based on the mathematical model in 3.2 it is possible to derive a location of the virtual origin based in Schlichting Schlichting (1968). Note that since this mathematical method contains possibilities for tilting the thruster an arbitrary angle α, the virtual origin may not necessarily be located along the axial centerline of the jet outlet. Thus the denotation s_0, which follows the path of the initial jet centerline upstream at arbitrary angles α, is chosen. See 3.6 for further explanation.

From 3.2 equation (3.19) is collected. The mass flux is defined as (C.37), and by introducing (3.19) and (C.20), (C.38) is obtained from the initial mass flux:

$$Q = \rho 2\pi \int_0^\infty ur \, \mathrm{d}r \tag{C.37}$$

$$Q = \rho 2\pi \frac{(s+s_0)^2}{A^2} \frac{3}{8\pi} \frac{K}{\epsilon_0 (s+s_0)} \cdot \int_0^\infty \frac{\eta \, \mathrm{d}\eta}{(1+\frac{1}{4}\eta^2)^2} \tag{C.38}$$

By introducing $u = \frac{1}{2}\eta^2$ it is possible to calculate the integral in the mass flux:

$$\int_0^\infty \frac{\eta \, \mathrm{d}\eta}{(1+\frac{1}{4}\eta^2)^2} = \int_0^\infty \frac{\mathrm{d}u}{(1+\frac{1}{2}u)^2} = -\frac{2}{1+\frac{1}{2}u}|_0^\infty = 2 \tag{C.39}$$

Thus, the mass flux (C.38) then becomes:

$$Q = (s+s_0) \cdot \frac{3}{2A^2} \cdot \frac{\sqrt{K}}{0.0161} \cdot \rho = 0.405 \cdot \sqrt{K} \cdot (s+s_0) \cdot \rho \tag{C.40}$$

Now, recalling 3.6 s_0 can be derived by looking at the slot, with boundary conditions $s = 0$ and $r = \frac{D}{2}$. K and Q are defined in C.30 and eq:Q respectively, both from Schlichting Schlichting (1968). Inserting the boundary values yields:

$$K = u_{ent}^2 \cdot \pi \cdot (\frac{D}{2})^2 \tag{C.41}$$

$$Q = \rho \cdot u_{ent} \cdot \pi \cdot (\frac{D}{2})^2 \tag{C.42}$$

which implies:

$$0.405 \cdot u_{ent} \cdot \frac{D}{2} \cdot \sqrt{\pi} \cdot s_0 \cdot \rho = \rho \cdot u_{ent} \cdot \pi \cdot (\frac{D}{2})^2 \tag{C.43}$$

$$s_0 = \frac{D}{2} \cdot \sqrt{\pi} \cdot \frac{1}{0.405} \tag{C.44}$$

From this, the location of the virtual origin, s_0, can be obtained:

$$s_0 = 2.18D \tag{C.45}$$

This is in fairly good congruence with the results of virtual origins from previous experimenters. There is, however, always uncertainties related to the actual location of the virtual origin, and the results should naturally be dealt with accordingly.

C.3 Lehn's deduction of jet entrainment

When assuming turbulent, stationary flow symmetric around the vector in the axial direction the Reynolds equations and the continuity equations can be written as in (C.46), (C.47) and (C.48). This following derivation sequence is found in Lehn Lehn (1985) and is also presented in the project thesis Fjørtoft prior to this master's thesis.

$$u\frac{\partial u}{\partial x} + v\frac{\partial u}{\partial r} = -\frac{1}{\rho}\frac{\partial p}{\partial x} + \nu(\frac{\partial^2 u}{\partial r^2} + \frac{1}{r}\frac{\partial u}{\partial r} + \frac{\partial^2 u}{\partial x^2}) - (\frac{\partial}{\partial r}\overline{u'v'} + \frac{\partial}{\partial x}\overline{u'v'} + \frac{\overline{u'v'}}{r}) \tag{C.46}$$

$$u\frac{\partial v}{\partial x} + v\frac{\partial v}{\partial r} = -\frac{1}{\rho}\frac{\partial p}{\partial x} + \nu(\frac{\partial^2 v}{\partial r^2} + \frac{1}{r}\frac{\partial v}{\partial r} - \frac{v}{r^2} + \frac{\partial^2 v}{\partial x^2}) - (\frac{\partial}{\partial r}\overline{v'}^2 + \frac{\partial}{\partial x}\overline{v'u'} + \frac{\overline{v'}^2}{r}) \tag{C.47}$$

$$\frac{\partial}{\partial r}(rv) + \frac{\partial}{\partial x}(ru) = 0 \tag{C.48}$$

Here u and r are the mean velocities in axial and radial direction, while u' and v' are the corresponding velocity fluctuations. Further p is the pressure, ν is the kinematic viscosity and ρ is the density of the fluid. Boundary layer theory is then used to further simplify these equations. The assumptions made are:

- $u >> v$
- $\frac{\partial}{\partial r} >> \frac{\partial}{\partial r}$
- The corresponding turbulent shearing forces are much larger than the viscous forces.

This eliminates the terms in (C.46), (C.47) and (C.48) multiplied with the kinematic viscosity ν, velocities and incremental change in velocities in radial direction and the incremental change in axial velocity $\frac{\partial}{\partial x}$. The simplified equations can then be expressed as:

$$u\frac{\partial u}{\partial x} + v\frac{\partial u}{\partial r} = -\frac{1}{\rho}\frac{\partial p}{\partial x} - (\frac{\partial}{\partial r}\overline{u'v'} + \frac{\overline{u'v'}}{r}) \tag{C.49}$$

$$\frac{1}{\rho}\frac{\partial p}{\partial x} = -(\frac{\partial}{\partial r}\overline{v'}^2) \tag{C.50}$$

$$\frac{\partial}{\partial r}(rv) + \frac{\partial}{\partial x}(ru) = 0 \tag{C.51}$$

The turbulent shearing stress τ, or Reynolds stress, is the dominant term in a turbulent boundary layer and is defined as follows:

$$\tau = \rho\overline{u'v'} \tag{C.52}$$

By shifting in the Reynolds stress in equation (C.49) and doing some manipulation gives the following equation:

$$u\frac{\partial u}{\partial x} + v\frac{\partial u}{\partial r} = \frac{-1}{\rho}\frac{\mathrm{d}p}{\mathrm{d}x} + \frac{1}{\rho r} + \frac{\partial}{\partial r}(r\tau) \tag{C.53}$$

Now, two new parameters need to be introduced in order to use Prandtl's mixing length theory Schlichting (1968). First, u_m is defined as the maximum velocity on the jet centerline and b is the radial distance in the jet where $u = \frac{u_m}{2}$. In addition the relation $\xi = \frac{r}{b}$ is defined. See Lehn's figure C.3 for further explanation.

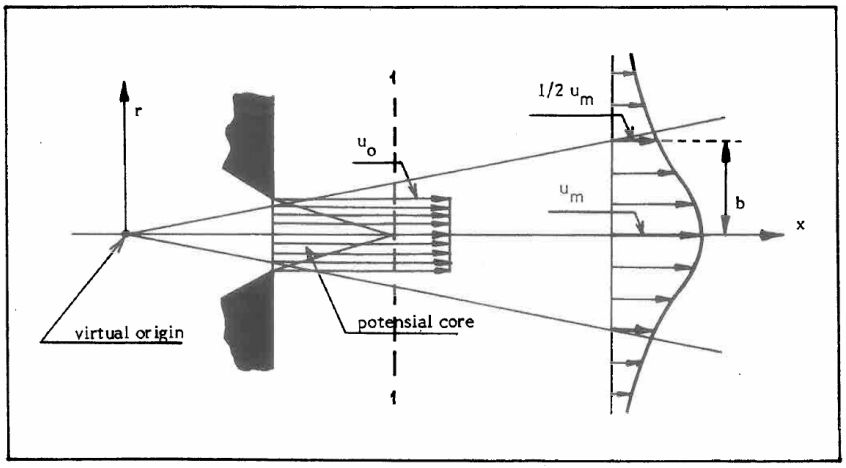

Figure C.3: Sketch of a free jet with corresponding bell shaped velocity distribution

Prandtl's mixing length theorem states for a circular turbulent jet, according to Schlichting Schlichting (1968) and Rajaratnam Rajaratnam (1976):

$$u_m \propto \frac{1}{x} \tag{C.54}$$

$$b \propto x \tag{C.55}$$

The Reynolds stress τ can be eliminated by two types of solutions according to Lehn Lehn (1985) and Rajaratnam Rajaratnam (1976); namely the Tollmien type solution and Goertler type solution. Both type solutions are described in Rajaratnam Rajaratnam (1976) for circular turbulent jets. Choosing the Goertler type solution the following velocity distribution can be found:

$$\frac{u}{u_m} = \frac{1}{(1 + (\sqrt{2} - 1) \cdot \xi^2)^2} \tag{C.56}$$

Having obtained the velocity distribution it is now possible to find the volume flow Q and the proportionality with x:

$$Q = \int_0^\infty 2\pi r u \,\mathrm{d}r \tag{C.57}$$

$$Q \propto x \tag{C.58}$$

Given that the axial momentum is preserved (C.58) shows that the jet must attract surrounding fluid as x increases downstream. This is what is known as entrainment. With a turbulent free circular jet symmetry around the centerline being assumed, the surrounding fluid is entrained into the jet stream from both sides Allery et al. (2002). However, when applying this on a

turbulent jet with a nearby wall downstream of the jet parallel to the centerline the surrounding fluid is free to be drawn to the jet stream on one side while the wall prevents new inflow of surrounding fluid on the "wall side" of the jet stream.

In the confined region between the jet and the wall, the surrounding fluid is accelerated near the solid wall and the pressure is reduced. This pressure drop induces the jet deflection towards the wall and attachment if the wall is long enough. The result is that this pressure drop deflects the jet stream towards the solid wall and induces the attachment of the jet stream on the wall. This behavior is also described in Fernholz Fernholz (1971) and Faltinsen Faltinsen (1990).

C.4 Deduction of numerical calculations

Having obtained an expression of the radius of the jet stream curve, R, in 3.28 this can now be used in the numerical solution. In C.4, collected from Faltinsen, all relevant parameters for the numerical solution are shown. When solving the force balance numerically r_0 is assumed to be small (i.e. a thin jet) and is neglected. Assuming this will result in the centerline of the jet being modeled instead of the outskirts of jet, meaning that the attachment length predicted is for when the jet centerline attaches to the wall. The spreading of the jet will be relatively large and result in the outskirts of the jet touching the wall before a significant part of the jet flow does. As seen in 3.28 the R takes on an imaginary value when $r_0 > h$, which result in corrupt values for the rest of the numerical simulation even though the deflected jet in practice has not caused a thrust loss at this stage. This assumption is not regarded as conservative, but will on the other hand both ease the calculations and the interpretation of the results.

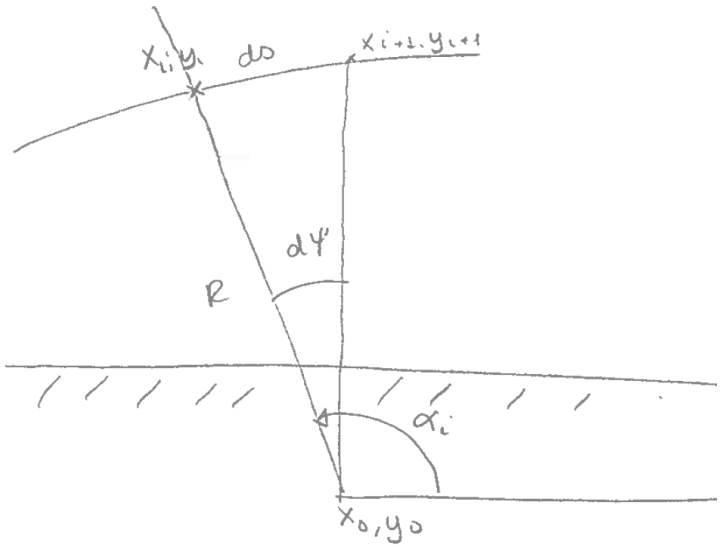

Figure C.4: Sketch of relevant parameters in the numerical solution

The incremental angle step is defined as $\mathrm{d}\psi = \frac{\mathrm{ds}}{R}$ given that $\tan \mathrm{d}\psi = \mathrm{d}\psi$ for small angles. The expressions for x_{i+1} and y_{i+1} are derived through C.65:

$$x_i = x_0 + R\cos\alpha_i \tag{C.59}$$
$$y_i = y_0 + R\sin\alpha_i \tag{C.60}$$
$$x_{i+1} = x_0 + R\cos\alpha_i - \mathrm{d}\psi \tag{C.61}$$
$$y_{i+1} = y_0 + R\sin\alpha_i - \mathrm{d}\psi \tag{C.62}$$
$$\Downarrow x_{i+1} = x_i - R\cos alpha_i + R\cos\alpha_i - \mathrm{d}\psi \tag{C.63}$$
$$y_{i+1} = y_i - R\sin alpha_i + R\sin\alpha_i - \mathrm{d}\psi \tag{C.64}$$
$$\tag{C.65}$$

The initial values are $\alpha_1 = \alpha + \frac{\pi}{2}$, $x_1 = 0$ and $y_1 = a$ also shown in 3.4.

Appendix D

Mathematical methods

D.1 Brix' mathematical method

The thrust deduction caused by the Coanda effect is graphically shown in D.1, and is divided into a primary and secondary thrust deduction ratio. The primary is caused by the deflection of the jet while the second is caused by additional friction. The jet can be deflected up to 90° at high ratios of surface radius to jet diameter or jet height, according to Brix Brix (1993).

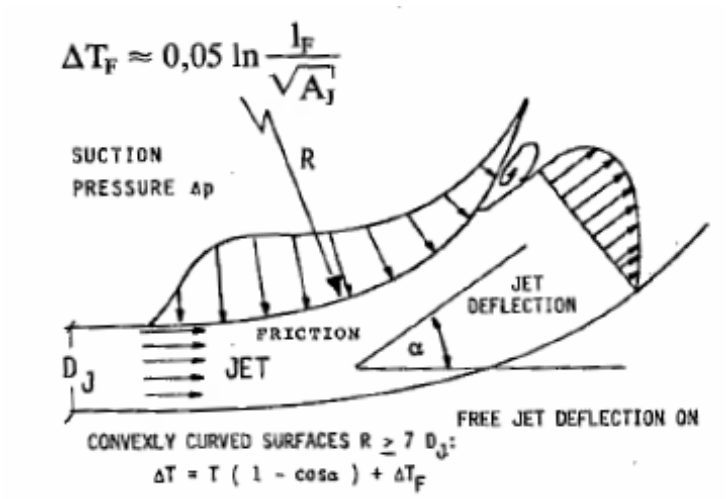

Figure D.1: Brix' thrust deductionby Coanda effect

The primary thrust deduction ratio is estimated by D.1:

$$T_C = T \cdot (1 - \cos \alpha_b) \tag{D.1}$$

where T_C is the primary thrust deduction ratio due to Coanda effect, T is the total thrust available and α_b is the deflection angle shown in D.1. The secondary thrust deduction ratio, which is due to friction losses, is roughly estimated in D.2:

$$\Delta T_F \sim 0.05 \ln \frac{l_F}{\sqrt{A_J}} \tag{D.2}$$

where ΔT_F is the secondary thrust deduction ratio, l_F is the friction length and A_J is the nozzle area, see D.1 for a further explanation of parameters. The total thrust deduction can then be estimated by adding the two contributions together:

$$\Delta T = T \cdot (1 - \cos \alpha_b) + \Delta T_F \tag{D.3}$$

D.2 Attachment length for various thruster angles of attack

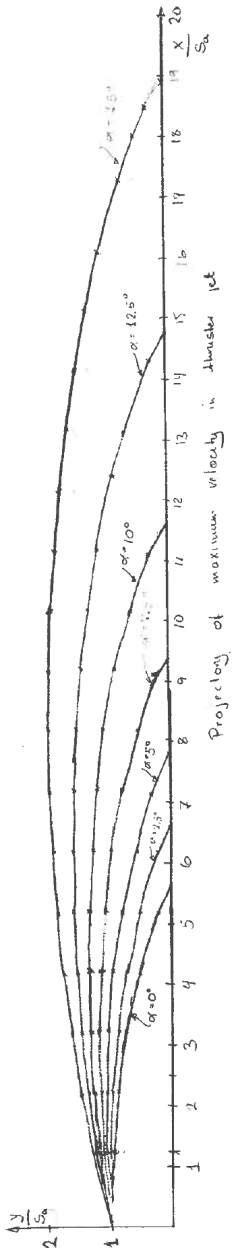

Appendix E

Inventory list of DVD

Pdf

1. The master's thesis "Thrust loss on azimuthing thrusters due to Coanda effect"

Matlab scripts

1. circ2.m - Which extracts the measured forces on the force transducers while the thruster rps is zero before and after the run is complete. Is used in correcting for circulation in the tank.
2. math.m - Which solves the force balance from Faltinsen's mathematical method in addition to processing the digitalized plotted hand written results attached in the unpublished notes.
3. decay.m - Which plots the responses and extracts the resonance frequency.

Footage

1. A short video clip of all runs at 17.5 rps.
2. Assorted illustration images of the model and experiment setup

Excel worksheets

1. Mean values.xlsx - Which contain all calculations performed in Excel. In general this worksheet contains all plots and calculations except those where the time series of the measurements are needed and the mathematical model.